THEME 9

Tubular Connections, Orthotropic Steel Decks

Assemblages de profils creux, tabliers métalliques orthotropes

Hohlprofilverbindungen, orthotrope Stahlfahrbahnplatten

Leere Seite

Blank page

Page vide

Ermüdungsverhalten geschweisster Hohlprofil-Fachwerkknoten aus Stahl

Fatigue Behaviour of Welded Joints in Trusses of Steel Hollow Sections

Comportement à la fatigue des assemblages soudés de poutres à treillis en profilés creux d'acier

F. MANG
Prof. Dr. -Ing.
Universität Karlsruhe
Karlsruhe, BRD

Ö. BUCAK
Dipl. Ing.
Universität Karlsruhe
Karlsruhe, BRD

ZUSAMMENFASSUNG
Die spezielle Problematik tragender Hohlprofile liegt im Bereich ihrer Anschlüsse und Verbindungen. Deshalb bedarf ihr Einsatz vorheriger eingehender Analysen zum Tragverhalten unter vorwiegend ruhender und schwingender Belastung. Im Knotenbereich geschweisster Hohlprofil-Fachwerkknoten treten inhomogene Spannungszustände auf, welche durch die Methoden der elementaren Festigkeitslehre nicht erfasst werden können. Untersuchungen zum Ermüdungsverhalten von K-förmigen Fachwerk-Knotenpunkten wurden durchgeführt. Über die Ergebnisse dieser Untersuchungen wird berichtet.

SUMMARY
Special problems arise in the areas of joints and connections of loadbearing hollow sections. Thus before specifying hollow sections the strength of the joints must be assessed for both dynamic and the predominant static loading. However, the non-homogeneous stress states which occur in the region of hollow section truss nodes cannot be analysed by methods of elementary strength theory. Studies of the fatigue behaviour of K-shaped truss nodes have been carried out and the results are presented in this paper.

RESUME
Les problèmes spécifiques aux profilés creux porteurs résident dans leurs zones d'assemblages. Leur emploi nécessite par conséquent des analyses préalables poussées de leur comportement aussi bien sous des charges statiques que dynamiques. Il se produit des états de contraintes inhomogènes dans la zone de tels noeuds soudés, qui ne peuvent être analysés par les méthodes élémentaires de la résistance des matériaux. Les résultats d'une recherche sont présentés dans le but de déterminer le comportement à la fatigue de noeuds d'assemblage de treillis en forme de K.

1. Parameter und Bezeichnungen

Die Definition der maßgebenden geome-
trischen Parameter von K-Knoten sind
Bild 1 zu entnehmen. Für Rund- und
Hohlprofil-Knoten gelten entspre-
chende Parameter.

2. Bruchfelder

Als Ergebnis Ergebnis einer umfas-
senden Literaturanalyse, welche
sämtliche verfügbaren Versuchs-
daten sowie eigene versuchstech-
nische Untersuchungen erfaßte,
wurden die Brucharten gemäß
Bild 2 gefunden. Ihre Abhän-
gigkeit von den maßgebenden Pa-
rametern ist in diesem Bild
dargestellt. Auf dieser Basis
wurde in Karlsruhe die "Bruch-
Kriterien-Methode" entwickelt.

Bei Knotenpunkten mit Spalt bzw.
geringen Überlappungsmaßen und
relativ kleinen Wanddicken-
Verhältnissen treten die Brü-
che in der Übergangszone der
Kehlnahtverbindung am Gurt-
stab auf. (Feld 1)
Werden an dem gleichen Knoten
alle Maße, mit Ausnahme der
Wanddicke des Gurtrohres, kon-
stand gehalten, tritt der
Bruch bei größerem T/t-Ver-
hältnis an der Zugdiagonale
auf, ausgehend von der Schweiß-
kerbe. (Feld 3) Dabei ist die
Bruchspannung (wie später er-
kennbar wird) in der Diagonalen
bei verschiedenen T/t-Verhält-
nissen konstant.

K - Knoten
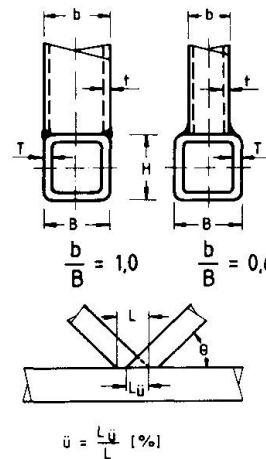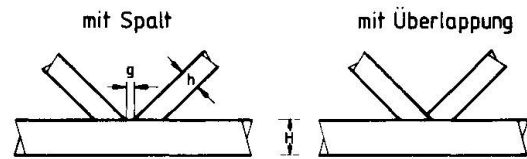
Geometrische Parameter

$\dfrac{b}{B}$ Breitenverhältnis

$\dfrac{T}{t}$ Wanddickenverhältnis

$\dfrac{g}{b}$ Spaltgröße

ü Überlappung

θ Systemwinkel

$\dfrac{B}{T}$ Breiten-Wanddicken-Verhältnis des Gurtstabes

$ü = \dfrac{L_{ü}}{L}$ [%]

$\dfrac{b}{B} = 1{,}0$ $\dfrac{b}{B} = 0{,}6$

Bild 1: Definition und geometrische Para-
meter bei Fachwerk-Knoten

$f_3 = g/d$ $D/T=20$ $\gamma = \dfrac{d}{D} = 0{,}75$ $\theta = 45°$

Bild 2: Brucharten bei Hohlprofil-Knotenpunkten

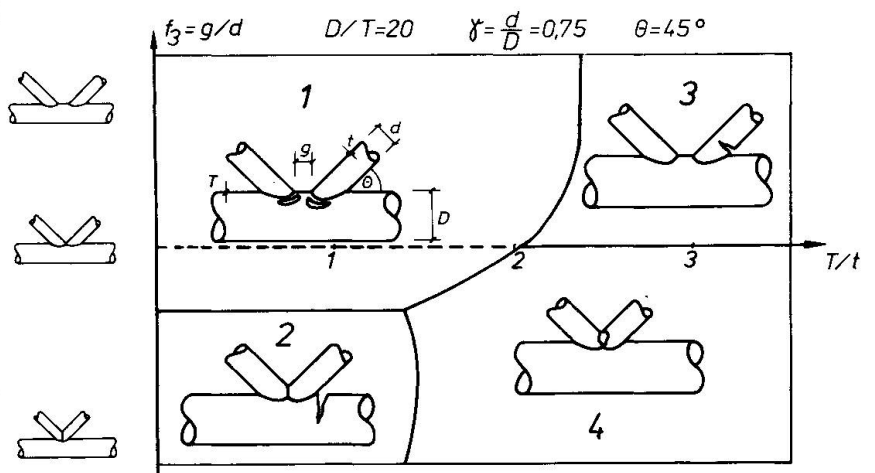Für größere Überlappungen und kleine T/t-Verhältnisse bricht der Gurtstab quer zur Längsachse des Gurtrohres. (Feld 2) Wird an dem gleichen Knoten die Wanddicke des Gurtstabes vergrößert, tritt der Bruch für den Fall gleicher Diagonalstababmessungen im Überlappungsbereich der Diagonalen auf. (Feld 4) In den Grenzbereichen der Bruchfelder sind Kombinationen dieser Brucharten möglich. Außer den hier kurz erläuterten Knotennachweisen muß für die Bruchfelder 1, 3 und 4 ein Nachweis zum Gurtstab unter Berücksichtigung der Schweißnahtkerbe durchgeführt werden.

3. Diagramme zum Knotennachweis

Auf der Basis der zuvorgenannten Analysen werden zur praktischen Anwendung Diagramme für Rund- und Rechteck-Hohlprofilknoten angeboten. Bild 3 zeigt die Diagramme für Rund- und Bild 4 für Rechteck-Hohlprofilknoten; weitere Diagramme können aus (1) entnommen werden. Als Bezugswert wird hier die Maximalspannung im Diagonalstab angegeben.

Aus diesen und ähnlichen Diagrammen können für bestimmte Durchmesser- bzw. Breitenverhältnisse in Abhängigkeit vom Wanddicken-Verhältnis und vom Spalt- bzw. Überlappungs-Verhältnis (ausgedrückt als g/b bzw. g/d) die ertragbaren Oberspannungen bei $2 \cdot 10^6$ Lastwechseln abgelesen werden. Die für Rund-Hohlprofilknoten aus diesen Diagrammen ablesbaren Werte gelten für eine 95 %ige Überlebenswahrscheinlichkeit und die für Rechteck-Hohlprofile für eine 50 %ige Überlebenswahrscheinlichkeit. Diese Werte müssen je nach Anwendungsfall mit einem Sicher-
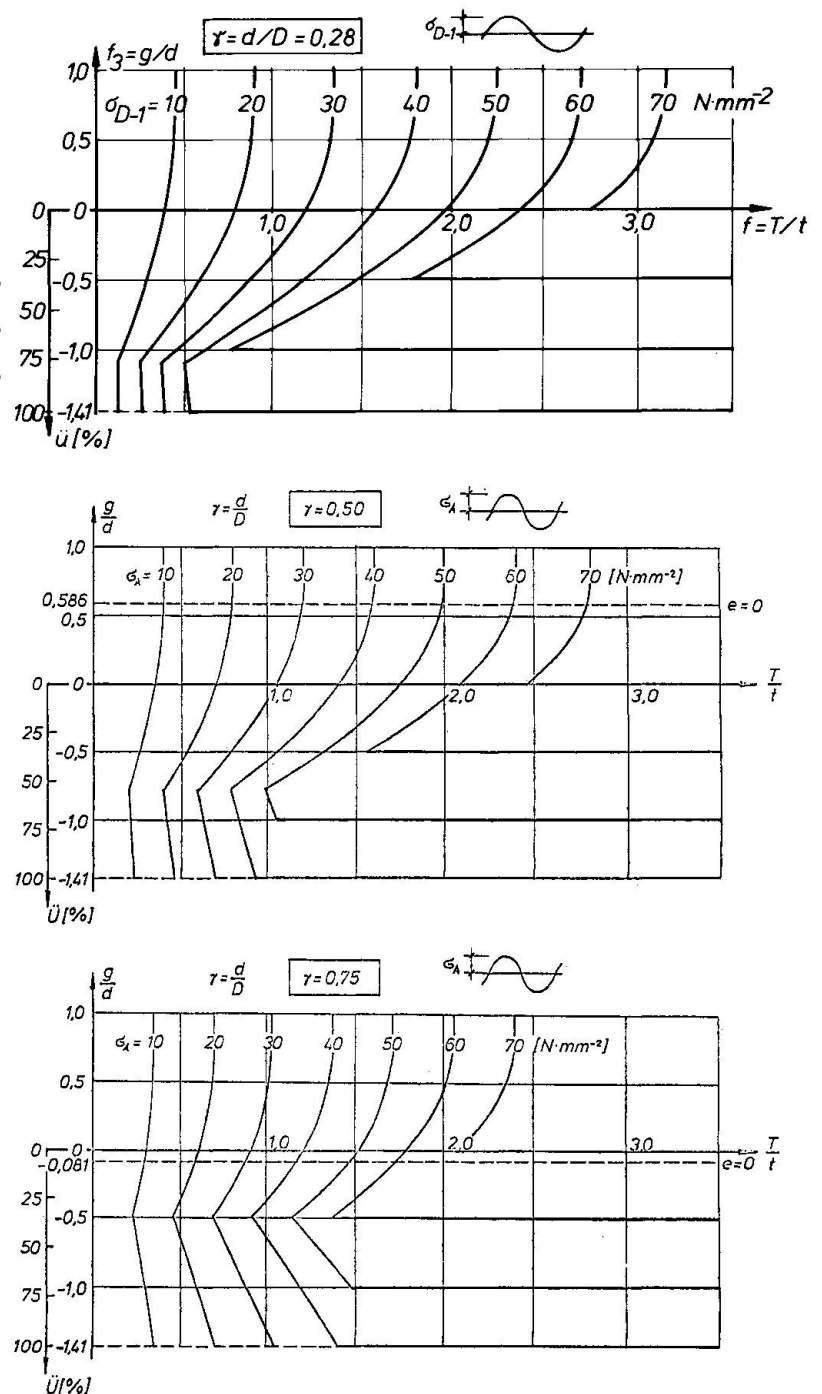
Bild 3: Bemessungsdiagramme für K-Knoten aus Rund-Hohlprofilen ($P_{ü}$ = 95 %)

heitsfaktor vermindert werden,
welcher z.B. zwischen 1,2 und
1,5 liegen könnte.

Für andere Grenzspannungsver-
hältnisse als R = -1 sowie für
den Zeitfestigkeitsbereich muß die
Diagonalspannung mit Hilfe dimen-
sionsloser Faktoren umgerechnet
werden. Hierzu können z.B. die
Formeln der DIN 15 018 ange-
wendet werden. Die Abweichungen
betrugen beim Vergleich mit
den Versuchswerten maixmal 12 %.
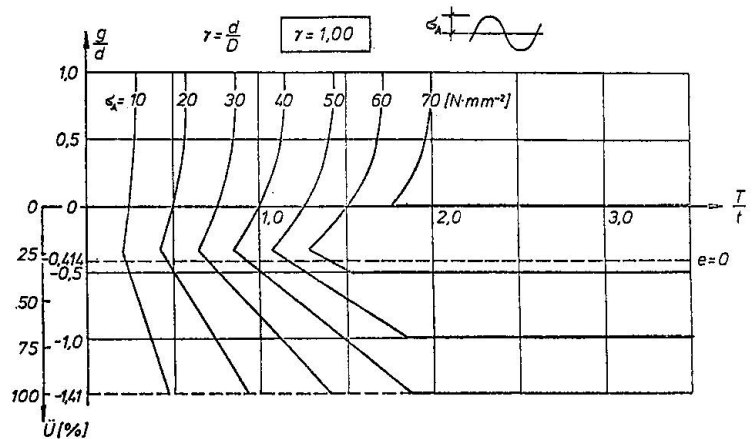
Noch zu Bild 3
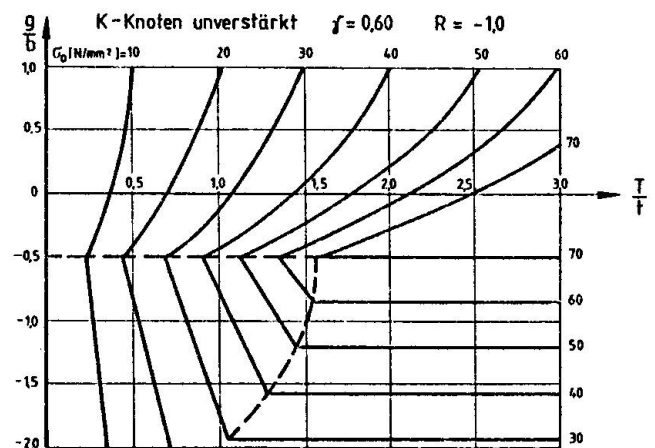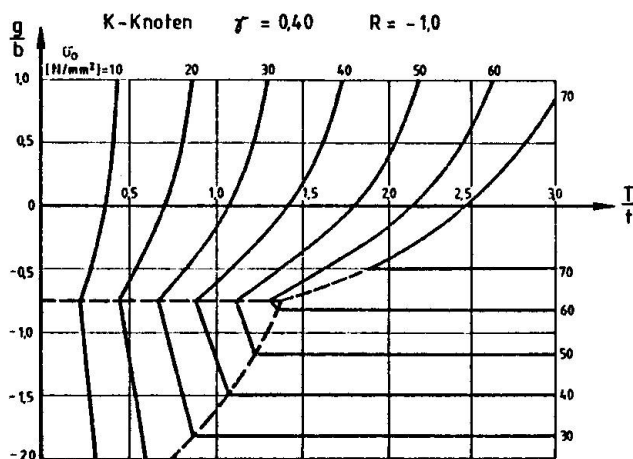
Bild 4: Bemessungsdiagramme für K-Knoten aus
Rechteck-Hohlprofilen ($P_ü$ = 50 %)

Die Umrechnung für den Zeitfestigkeitsbereich erfolgt über die unten angegebene
Formel:

$$\log.\ \sigma_{max,nenn} = \frac{6,3 + K \cdot \log \sigma_{Diagr} - \log N_B}{K}$$

Darin bedeuten:

K .... Maß für die Steigerung der Wöhlerlinie

σ_{Diagr} ..... Oberspannung aus dem Bemessungsdiagramm für $2 \cdot 10^6$ Last-
wechsel bei R = -1,0

N_B .... erwartete Lastspielzahl

$\sigma_{max,nenn}$ .. maximal zulässige Nennspannung für die Lastwechselzahl N_B

Die K-Faktoren können in Abhängigkeit von der Geometrie und vom Werkstoff aus der unten angegebenen Tabelle entnommen werden.

| Werkstoff | K-Faktoren | | | |
| | Rund-Hohlprofile | | Rechteck-Hohlprofile | |
	Spalt	überlappt	Spalt	überlappt
St 37	5,0	6,5	5,0	4,0
St 52	4,5	6,0	5,0	4,0
St E 690	4,0	5,5	--	--

Die Grenzen der einzelnen Brucharten verlagern sich in Abhängigkeit vom Durchmesserverhältnis d/D. Außerdem ist damit die Höhe der ertragbaren Dauerschwingspannung unterschiedlich.

4. Fachwerkknoten mit örtlichen Verstärkungen

B.... Breite des Gurtstabes
b.... Breite der Diagonalen bzw. Vertikalen
T.... Wanddicke des Gurtstabes
t.... Wanddicke des Diagonalstabes
L_D... 2·√2·b + g
L_S... Länge des Versteifungsbleches
t_S... Dicke des Versteifungsbleches
b_S... Breite des Versteifungsbleches
g.... Spalt

b_S... Breite des Versteifungsbleches
t_S... Dicke des Versteifungsbleches

Detail A1
ohne Schweißnaht

Detail A2
mit Schweißnaht

Detail A1
ohne Schweißnaht des Versteifungsbleches

Detail A2
mit Schweißnaht des Versteifungsbleches

Erläuterung der Bezeichnungen siehe Versteifungsart 1 und 2

t_{S1}.... Dicke des horizontalen Versteifungsbleches
t_{S2}.... Dicke des vertikalen Versteifungsbleches
b_{S1}.... Breite des horizontalen Versteifungsbleches
b_{S2}... Breite des vertikalen Versteifungsbleches

Versteifungsart 2

Versteifungsart 1
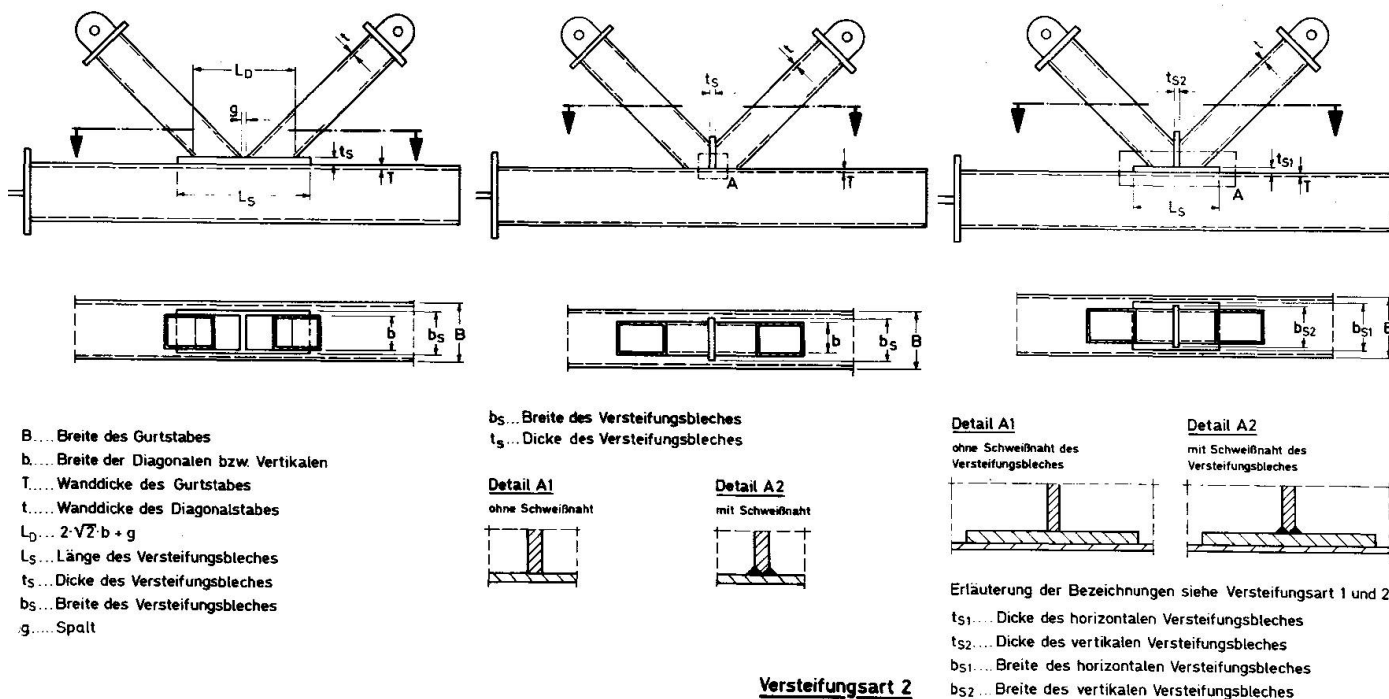
Versteifungsart 4

Bild 5: Versteifungsarten mit den zugehörigen maßgebenden Parametern

Die vorgestellten Bemessungsdiagramme für Rund- und Rechteck-Hohlprofile sind nur zutreffend für unmittelbar miteinander verschweißte Rohre.

Zur Steigerung der Zeit- und Dauerfestigkeit von Rechteck-Hohlprofil-Knotenpunkten kommen verschiedene Versteifungsarten in Betracht (siehe Bild 5).

Von diesen Versteifungsarten wurde die Form 1 bis jetzt ausführlich untersucht.
Die Bilder 6 und 7 geben entsprechende Wöhlerlinien vergleichend wieder.

Die Steigerung der Zeit- und Dauerfestigkeit für die Versteifungsart 1 ist in den Bildern 6 und 7 in Abhängigkeit von der Dicke des Versteifungsbleches im Vergleich mit einem unausgesteiften Knotenpunkt zu entnehmen.

Bild 6: Steigerung der Zeit- und Dauerfestigkeit mit zunehmender Verstärkungs-Blechdicke

Solche Versteifungsarten werden insbesondere im Bereich der Auflager angewandt, wo aus statischen Gründen größere Diagonalkräfte und kleinere Gurtkräfte auftreten. Dies führt zu einer wirtschaftlichen Bemessung solcher Fachwerke.
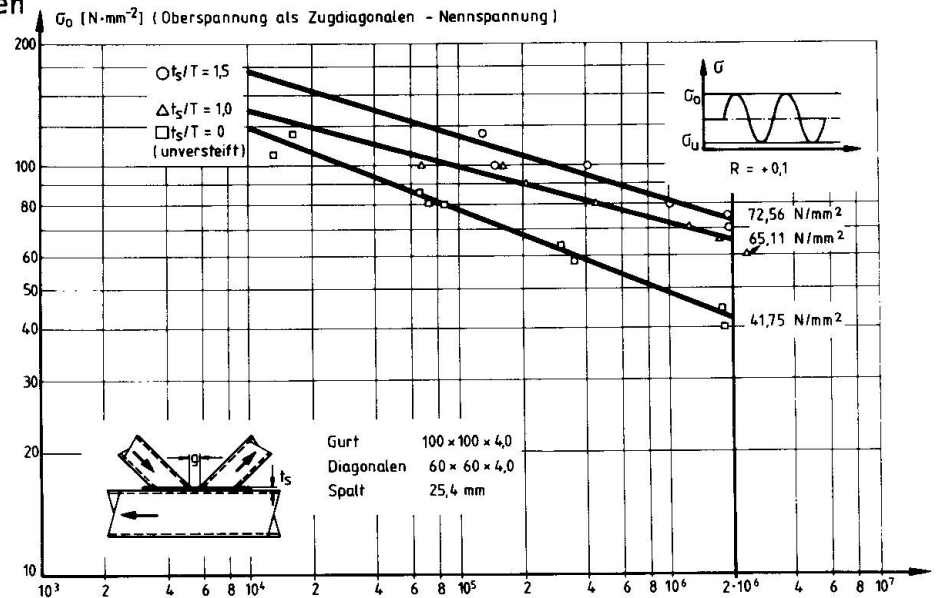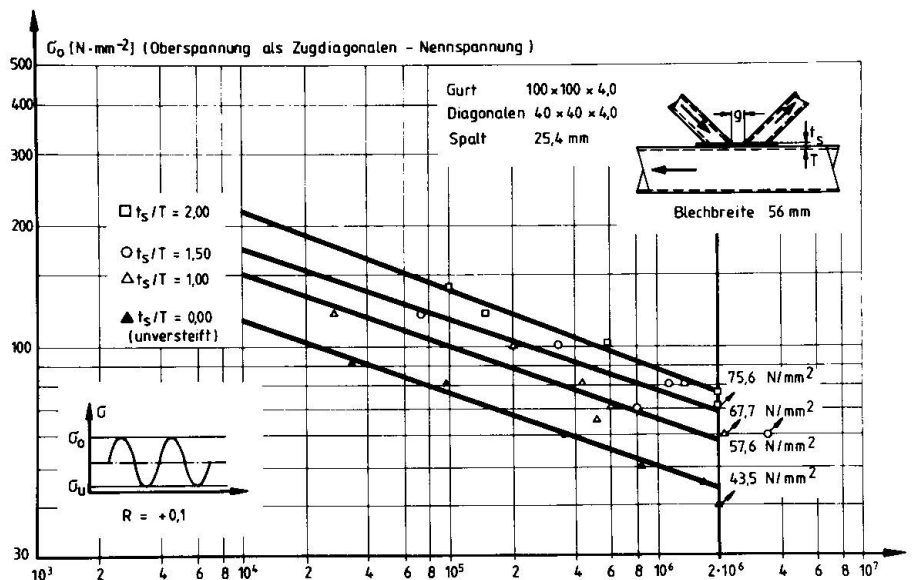
Bild 7: Steigerung der Zeit- und Dauerfestigkeit mit zunehmender Verstärkungs-Blechdicke

Die Wahl der optimalen Ver-
stärkungsblech-Länge und
Breite wird z.Zt. unter-
sucht. Aus Bild 8 geht z.B.
hervor, daß bei einem Brei-
tenverhältnis b/B = 0,4
eine Verstärkungsblechbreite
von 56 mm höhere Zeit- und
Dauerfestigkeitswerte lie-
fert als jene mit 80 mm.
Dies ist auf die wachsen-
de "Weichheit" des Aus-
steifungsbleches mit zu-
nehmender Breite zurück-
zuführen. Es werden näm-
lich die Zusatzbiegungen
infolge der Verformungen
des Aussteifungsbleches
größer.

Eine kurze Versteifungs-
blechlänge ist gemäß
Bild 9 im Falle des Knotens
mit Spalt vorteilhaft.

Ab einem bestimmten Län-
genmaß für das Verstei-
fungsblech ist kein Ein-
fluß mehr feststellbar. Bei
überlappten Knotenpunkten,
die in unversteifter Aus-
führung durch Gurtbrüche
(Bruchart 2 gem. Bild 2)
quer zur Gurtlängsachse
versagen, wird sich durch
diese Versteifungsart und
größere Blechlängen eine
Zeit- und Dauerfestigkeits-
steigerung erreichen las-
sen. Dabei wird nämlich
im kritischen Bereich
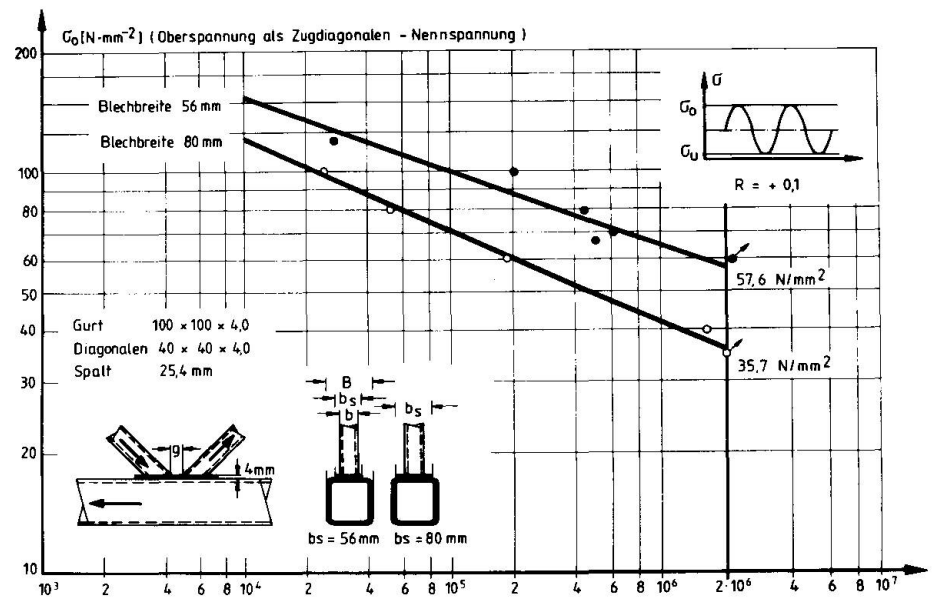
Bild 8: Einfluß der Blechbreite auf die Zeit- und
          Dauerfestigkeit
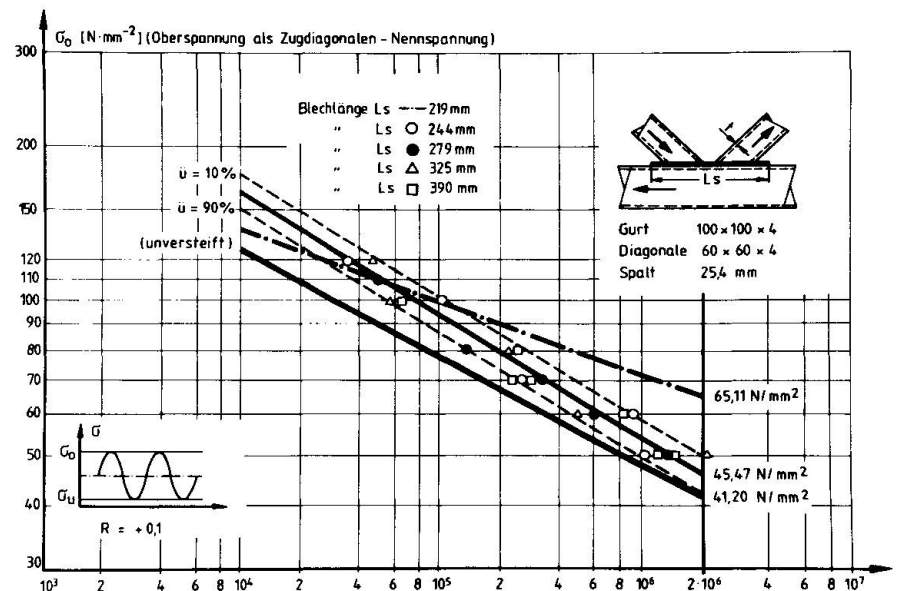
Bild 9: Einfluß der Blechlänge auf die Zeit-
          und Dauerfestigkeit

anstelle einer Quernaht eine
durchlaufende Längsnaht vor-
liegen und die im Knoten-
bereich maßgebenden Bean-
spruchungen durch die zu-
sätzliche Versteifungs-
platte abgemindert werden.

Die zusätzliche Erhöhung
der Zeit- und Dauerfestig-
keit durch die Versteifungs-
art 4 ist im Vergleich mit
den Daten zur Versteifungs-
form 1 in Bild 10 erkenn-
bar.
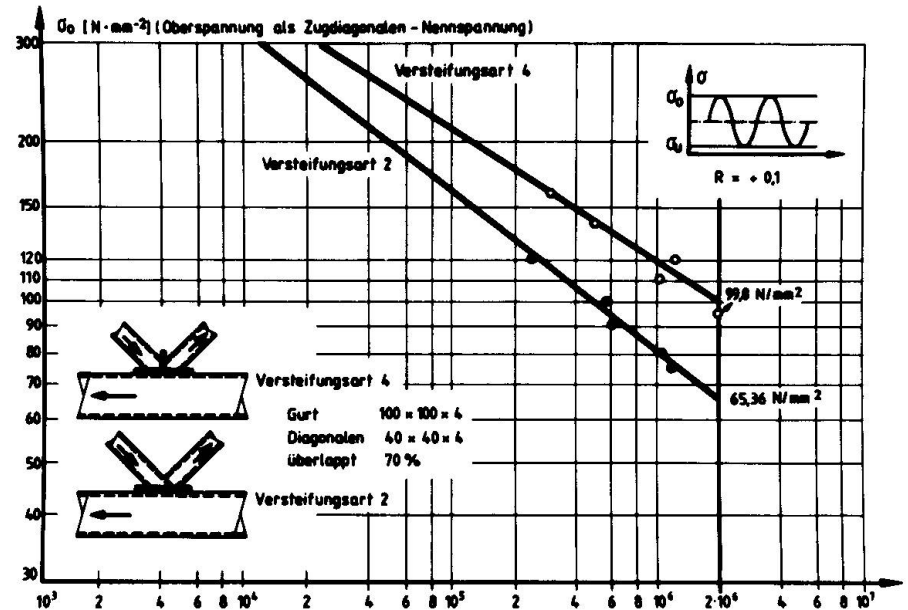
Bild 10: Vergleich verschiedener Versteifungsarten

Daß die gleichen Tenden-
zen bei den verstärkten
Knotenpunkten wie bei den
unverstärkten Knoten be-
züglich der Auswirkung
von Oberlappungen gelten
(g/b-Verhältnis), ist
aus dem Bild 11 erkennbar.
Eine 70 %-Oberlappung ist
nicht günstiger als jene
mit 37 % Oberlappung.
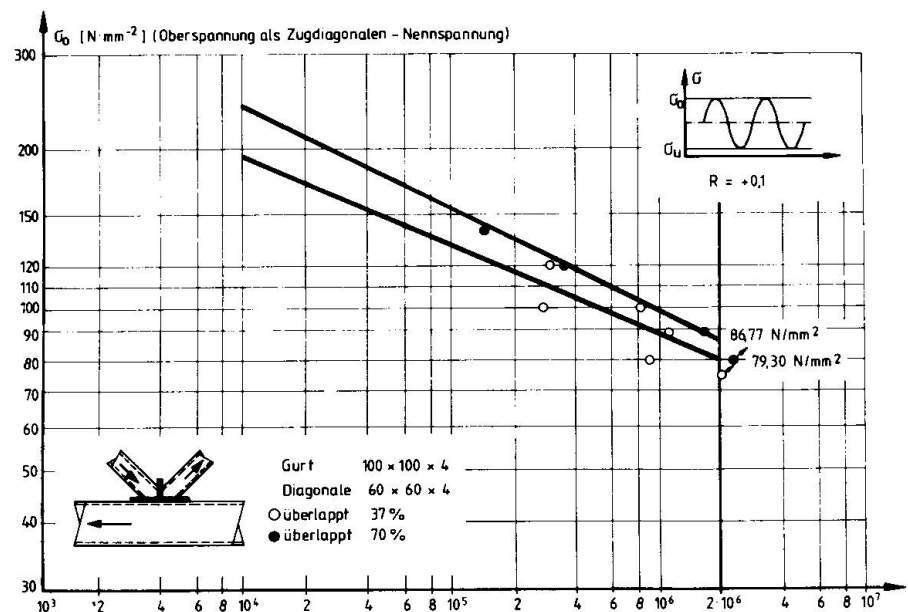
Bild 11: Auswirkungen von Oberlappungsverhältnissen
auf die Zeit- und Dauerfestigkeit von
Knotenpunkten, verstärkt gemäß Form 4

5. Anwendungsfälle

Die vorgestellten Bemes-
sungsgrundlagen konnten
in den letzten Jahren mehr-
fach angewendet werden.
Einige Bauwerke werden
nachfolgend vorgestellt:

5.1 Lion's Gate Bridge in Vancouver-Canada

Die Hauptträger dieses teil-
weise zu erneuernden Bau-
werkes sind als Fachwerk-
träger,mit aus Blechen zu-
sammengesetzten Kastenträ-
gern als Gurte, ausgebil-
det. Die Füllstäbe sind
Rechteck-Hohlprofile. Die
Knotennachweise wurden
nach der behandelten
Bruch-Kriterien-Methode
geführt. Die Schweiß-
nähte der Gurte wurden
zusätzlich untersucht.
Danach ergab sich, daß die
Schweißnahtausführung nach
Detail F auch für Detail E
ausreichend ist, wenn
wegen der Terrassenbruch-
gefahr des Stegbleches die
Knotenvorbereitung am Steg-
blech ausgeführt wird. Die
Schweißnahtdetails der Kno-
tenpunkte sind dem Bild 13
zu entnehmen.

LION'S GATE BRIDGE
IN VANCOUVER

Bild 12: Gesamtansicht und Querschnitt der Brücke

Schnitt A-B

Detail A   Detail B   Detail C

Detail D   Detail E1   Detail E2   Detail F
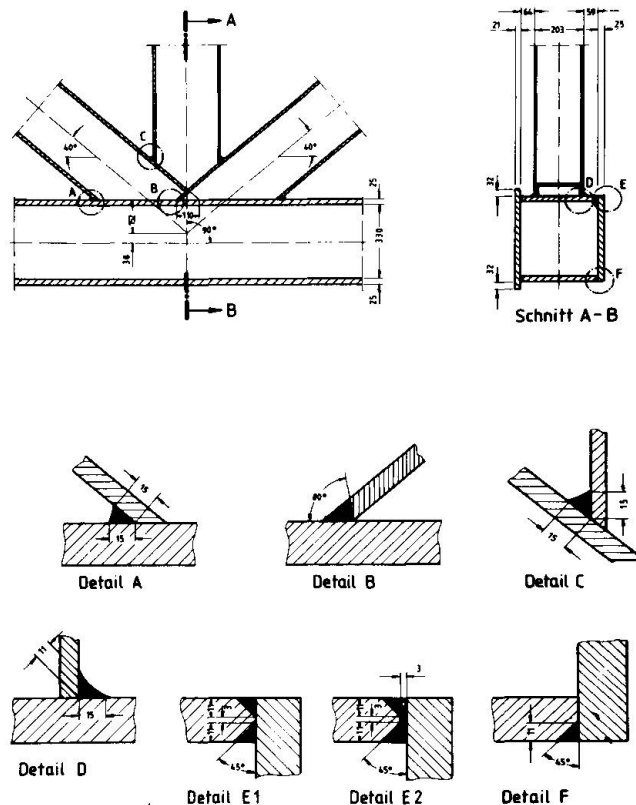
Bild 13: Die ursprünglichen Schweißnahtdetails
der Brücke

5.2 Überdachung des Flugzeughangars Singapur

Die größte Überdachung für einen Flugzeughangar ohne Zwischenstützen, mit den Grund-
rißabmessungen von ca. 220 m x 100 m wurde aus Rund-Hohlprofilen gebaut. Das statische
System ist durch einen Diagonalrost gebildet, welcher im Bereich der großen Öffnung
von einem räumlichen Randträger gestützt ist. Da am Dach verschiedene bewegliche Kran-
anlagen und Wartungsplattformen montiert sind, wurde das Bauwerk für eine Lastwechsel-
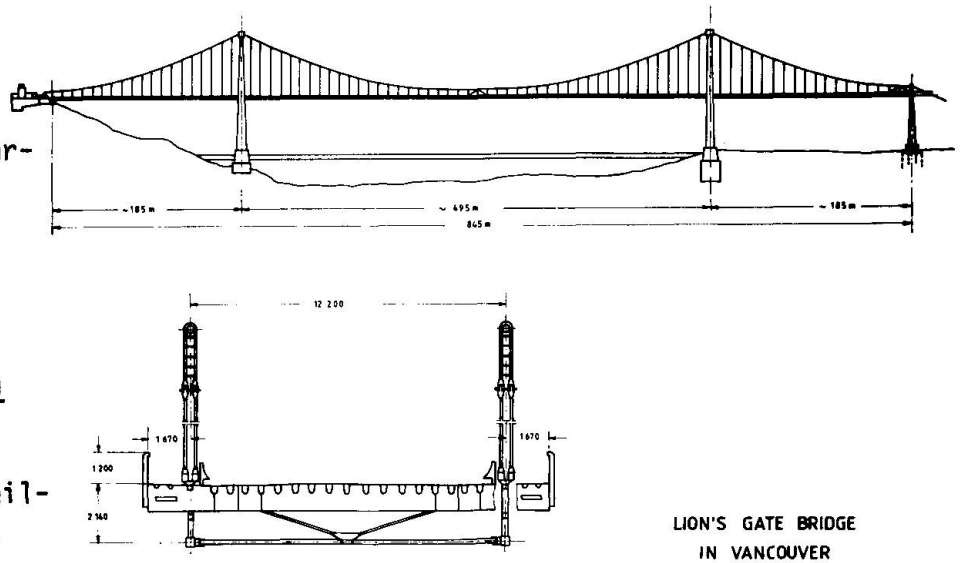zahl von 100.000 der Maximalgröße bemessen. Die größten Rohrabmessungen des Daches, im
Bereich der großen Seitenöffnung betragen Ø 813 x 60 mm. Das Bild 14 zeigt dieses Dach
im Vormontagezustand in Bodennähe. Nach Fertigstellung ist die Anhebung in die Endpo-
sition vorgesehen.
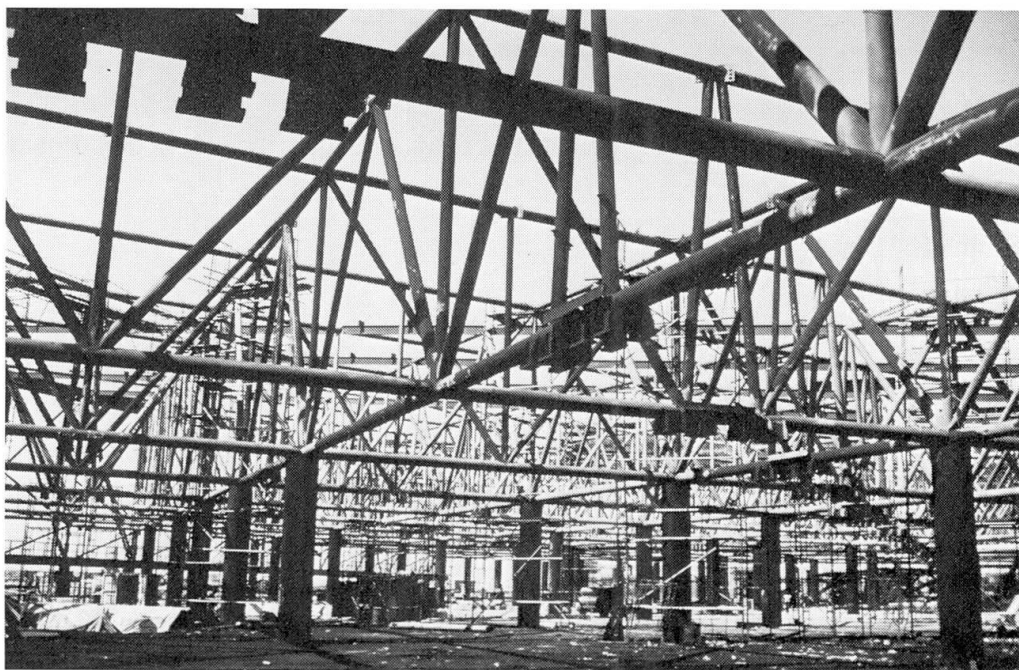
Bild 14: Montagezustand; das Dach liegt auf den Hilfsstützen

Literatur

1) Mang, F., D. Dutta und J. Wardenier: "Schwingfestigkeitsverhalten geschweißter
       Hohlprofilverbindungen". Herausgeber: Beratungsstelle für Stahlver-
       wendung, Düsseldorf, November 1981, ca. 400 Seiten

2) Mang, F., J. Wardenier, Ö. Bucak und D. Dutta: "Zeit- und Dauerfestigkeit von
       einfachen geschweißten Fachwerkknoten aus Rund-Hohlprofilen". November 1980
       Herausgeber: Studiengesellschaft für Anwendungstechnik von Eisen und
       Stahl e.V., Düsseldorf

3) Mang, F. : Abschlußbericht zum Forschungsvorhaben "Untersuchungen an Knotenpunkten
       aus Rechteck-Hohlprofilen mit örtlichen Verstärkungen".(unveröffentlicht)
       AIF-Nr. 4133, DVS-Nr. 9.078, März 1981

Fatigue Tests on Rectangular Hollow Sections: Truss Joints

Essais de fatigue sur des sections creuses rectangulaires: assemblages dans les treillis

Ermüdungsversuche an Rechteckrohren: Fachwerkknoten

R.B. OGLE
MHBH Consulting Engineers, Ltd.
Edmonton, AB, Canada

G.L. KULAK
Professor
University of Alberta
Edmonton, AB, Canada

SUMMARY
Fatigue tests were carried out on nine full-size trusses made from rectangular hollow sections. Two K-joint configurations were examined, gap and overlap. Three trusses were of cold-formed steel and six were of hot-formed steel. Both the tests and finite element analyses showed that testing joints in isolation may give fatigue strengths which are greater than testing the same joints in trusses. For these K-type joints, overlap joints performed better than gap joints. The use of hot-formed steel did not affect the results.

RESUME
Des essais de fatigue ont été effectués sur neuf treillis en vraie grandeur composés de barres à sections creuses et rectangulaires. Deux assemblages de type K ont été examinés. Trois treillis étaient en acier écroui à froid et six étaient en acier formé à chaud. Les essais aussi bien que les analyses par éléments finis ont montré que l'essai des assemblages peut donner des résistances à la fatigue supérieures à celles des mêmes assemblages essayés dans les treillis. Les assemblages dont les barres se recouvrent, se comportent mieux que ceux ayant un espace entre les barres. L'utilisation d'aciers différents n'a pas influencé les résultats.

ZUSAMMENFASSUNG
An neun Fachwerkträgern aus Rohren mit rechteckigem Hohlquerschnitt wurden Ermüdungsversuche durchgeführt. Zwei Typen von K-Verbindungen wurden geprüft. Drei Träger bestanden aus kaltverformten und sechs aus warmgewalzten Profilen. Die Versuche wie auch eine Finite-Element-Berechnung zeigten, dass isolierte Knotenverbindungen grössere Ermüdungsfestigkeiten ergeben können als Versuche an gleichen Knoten in einem Fachwerk. Knoten mit sich übergreifenden Streben verhielten sich besser als solche mit einem Zwischenraum zwischen den Streben. Die Stahlsorten haben die Versuchsresultate nicht beeinflusst.

1. INTRODUCTION

Because of their excellent structural properties, hollow structural sections (HSS) of either hot-formed or cold-formed structural steel are finding in-creased use in civil engineering structures. These sections can be either circular (CHS) or rectangular, including square, (RHS). Although combinations of these types can be found in trusses, only those cases with rectangular sections as both chord and web members will be discussed herein. The objective of the study was to investigate the fatigue behavior of trusses made from RHS, especially those involving K-type joints. The detail examined included both overlap and gap joints.

A review of some current North American [1,2], British [3], and European [4] specifications indicates that none specifically include design rules for the fatigue strength of HSS joints. The ECCS draft document on fatigue [5] like-wise does not yet include this detail. Design procedures are set forth for circular-to-circular tube connections as found in offshore structures [6]. This involves prediction of hot-spot stresses by a finite element analysis, calculation of the stress concentration factor (SCF), and then comparison with the fatigue life of the appropriate weld type.

Previous investigations of the fatigue strength of hollow structural sections have been conducted in Europe [7], Great Britain [8], and Japan [9]. Mainly because of the expense involved, most of these investigations have been carried out on isolated joints. In addition, the "chord" portion of the joint was in compression in many of the tests, apparently as a convenience in arranging the test set-up. The tests reported in this study were all carried out on joints contained within full-size trusses so that the effect of secondary bending moments might be examined. As well as obtaining the test results, a finite element analysis was used to predict hot-spot stresses.

2. FACTORS AFFECTING FATIGUE STRENGTH

Stress range, number of load applications, and the type of detail are usually sufficient to predict the fatigue strength of welded steel structures [10]. The flaw size, weld profile, and geometrical properties of the critical region are not explicitly considered since they are contained within the type of detail being tested. HSS joints contain even more geometrical factors than usual for welded details. These include the ratios of web member width to chord width, web member wall thickness to chord member wall thickness, chord wall thickness to width, and the amount of gap or overlap at the intersection of the web members and chord. Because of the large number of geometrical variables possible, only gap and overlap joints were examined in this study. Fig. 1 defines gap and overlap.

3. EXPERIMENTAL PROGRAM

Nine full-size trusses were tested. The general configuration and geometry are shown in Fig. 2. The critical joint was expected to be L1 where the K-joint was either gap or overlap. In all cases, the lower chord was an HSS 152.4 x 101.6 x 6.35 and the web diagonals framing into Joint L1 were each HSS 88.9 x 88.9 x 4.78. Test Series 1 (TS1) comprised three identical trusses made from hot-formed steel (nominal yield 350 MPa). The K-joint L1 was over-lapped 40%, with resulting zero joint eccentricity. Test Series 2 (TS2) was identical to TS1 except that cold-formed steel was used. Test Series 3 (TS3) had similar overall geometry to the first two series, used hot-formed sections,

but had gapped joints. The amount of the gap was 30 mm, and the resulting eccentricity was 43 mm. In the case of the gap joints, fillet welds were used to attach the web members to the chord face. In the overlap joints, fillet welds were used at the web-to-chord intersections and a full penetration groove weld, including backing bar, used where the web members met one another.

The stress range for the joint was defined as that present in the tension diagonal (L_1U_2). It was established under actual loading conditions using strain gages on the member. Strain gages were used to measure local stresses in the region of the joint. They were also placed on the member in such a way as to measure bending stresses throughout the truss.

Failure in a joint was considered to have occurred when approximately one-quarter of the cross-section L1-U2 had cracked through.

4. TEST RESULTS

4.1 Secondary Stresses

Practically all previous fatigue testing of HSS joints has been conducted on isolated specimens acting under axial forces only. This corresponds to the member forces that would be obtained from an analysis of the structure assuming pinned connections. Obviously, such an analysis disregards the presence of bending moments and shears which exist in the real structure as a result of joint fixity. Part of the purpose of this study was to see whether these effects have an important influence on fatigue life. In addition, analytical methods which attempt to predict these secondary effects were examined.

A direct stiffness program was used to analyze the trusses. The accuracy of the method in predicting the measured bending stresses in a typical member which frames into joint L1 can be seen in Fig. 3. This is considered typical. The measured maximum bending stress was 19%, 48% (chords), 21%, and 33% (web members) of the nominal axial stress for the four members which frame into joint L1 of TS3 (gap joint). It is likely, therefore, that secondary stresses were important in the fatigue life of these trusses. Secondary stresses were not measured in series TS1 and TS2 but they would not have been as significant since joint L1 had zero eccentricity in those trusses.

4.2 Crack Initiation and Growth

In all three test series, cracking was observed in the lower K-type joint L1, and in six of the nine trusses failure occurred at this joint. In the other cases, failure occurred at the upper K-joint, U2. The fatigue lives of all specimens are shown in Fig. 4.

In both Test Series 1 and 2 (overlap joints), cracking initiated in the vicinity of the groove weld. The cracks grew downward into the fillet welds, and at a later stage, separate cracks started at the fillet welds on the acute angle side of the web members. In Test Series 3 (gap joints), cracking started at the toe of the fillet weld where the front of the tension web member joined the top of the chord. Eventually, the cracks were always aligned transverse to the longitudinal axis of the tension member.

4.3 Measurement of Local Stresses

The test program allowed measured stresses in the joint region to be compared with those calculated using a finite element analysis. The loading for the

finite element analysis included the case of axial load only, and this allowed examination of past testing in which the "chord" of an isolated joint was in compression. The general load case used permitted input of either measured or theoretically calculated member axial forces, moments, and shears.

The theoretical analysis showed that chord precompression has a significant effect on the stresses in the gap region of gap joints. Changing the chord force from compression to tension increased the maximum principal tension stress in the gap by a factor of about 1.4. There are test results that support this conclusion [11]. The same increase was not present in overlap joints, however. In the overlap joints tested, force transfer was mainly through the sidewalls of the diagonals.

The effects of moment and shear in the truss members on the stresses in the joint region were different for gap and overlap joints. In the former, the principal tension stress increased by a factor of about 1.45 in the most highly stressed element. In the overlap joint, at least for this geometry, the finite element model showed that stresses in the crotch of the joint, where the fatigue cracks did initiate, did not increase appreciably when moments and shears were included. The experimental strains obtained in these tests were not consistently useful for comparison with measured strains. However, very short gages placed very close to the fillet weld toes in the gap joints did show strains consistent with calculated values.

4.4 Fatigue Strength Results

The results of all three series in this program are shown in Fig. 4. Also shown are data provided by Mang [12] from tests on isolated K-type joints. Although the latter do not have the same dimensions as the specimens in this study, the important non-dimensional parameters are very similar. It can be seen that the isolated joint data generally plots above the data obtained from complete trusses, and this indicates that isolated joints may have a higher apparent fatigue strength. This could be due either to the effect of secondary bending in the truss specimens or, perhaps, to the fact that the isolated joints had precompressed chords.

Although there are not many data points, the test results reported in this study indicate that (1) fatigue life is not significantly influenced by differences between hot-forming or cold-forming of the members, and (2) gap-type K joints have a lower fatigue resistance than overlap-type K joints. Shown in Fig. 4 for purposes of comparison is the most restrictive fatigue resistance curve now prescribed in North America for welded details [2].

Another way of examining the results is to apply a stress concentration factor (SCF) to the nominal axial stress range. This SCF should account for the secondary stresses due to moment and shear, and, perhaps, the effect of the weld profile. For the gap joints tested in this study, this approach gave reasonable, but unconservative, agreement with the fatigue strength of welds alone. For the overlap joints, the use of a SCF showed good correlation (slightly conservative) when compared to the weld strength.

5. SUMMARY AND CONCLUSIONS

Tests were conducted on nine full-size trusses made of rectangular HSS steel members in order to assess the fatigue strength of the K-joints. Both overlap and gap joints were examined, and both cold-formed and hot-formed tubes were used. The effect of secondary stresses due to moments and shears in the truss

members was evaluated both analytically and experimentally. The results are compared to tests on similar joints which were tested in isolation. Based on these tests, the following conclusions can be stated:

- there are no significant differences in fatigue strength with respect to the use of hot-formed or cold-formed sections.
- for K-type joints, overlap joints perform better in fatigue than do gap joints.
- testing HSS joints in isolation may give fatigue strengths which are greater than testing the same joints in trusses.
- the effects of the secondary moments and shears which are present in actual trusses result in significantly higher stresses than nominal for gap-type K-joints. There does not seem to be a significant increase for overlap joints when the joint eccentricity is zero, however.

REFERENCES

1. Canadian Standards Association, Standard S6-1974, Design of Highway Bridges, Rexdale, Ontario, 1974.
2. American Association of State Highway and Transportation Officials, Standard Specification for Highway Bridges, Twelfth Edition, Washington, D.C., 1977.
3. British Standards Insitution, Steel, Concrete and Composite Bridges: Part 10 Code of Practice for Fatigue, BS 5400, London, England, 1980.
4. Schweizerischer Ingenieur-und Architektenverein, SIA Standard 161, Steel Structures, Zurich, 1979.
5. European Convention for Constructional Steelwork, Recommendations for the Fatigue Design of Structures, Second Draft, 1981.
6. Marshall, P.W., Basic Considerations for Tubular Joint Design in Offshore Construction, Bulletin 193, Welding Research Council, New York, N.Y., 1974.
7. Mang, F., and Datta, D., Fatigue Strength of Welded Joints of Hollow Sections, Symposium on Tubular Structures, Delft, Netherlands, October, 1977.
8. Eastwood, W., Osgerby, C., Wood, A.A., and Babiker, D.B., Fatigue Behaviour of Welded Joints Between Structural Hollow Sections, University of Sheffield, Sheffield, England, 1970.
9. Kurobane, Y., and Konomi, M., Fatigue Strength of Tubular K-Joints, S-N Relationships Proposed as Tentative Design Criteria, IIW Document XV 340-73, 1973.
10. Fisher, J.W., Fatigue Strength of Welded Steel Details and Design Considerations, Proceedings, Canadian Structural Engineering Conference, Montreal, 1972.
11. Maeda, T., Uchino, K., and Sakurai, H., Experimental Study on the Fatigue Strength of Welded Tubular T and X Joints, IIW Document No. XV 270-69, 1969.
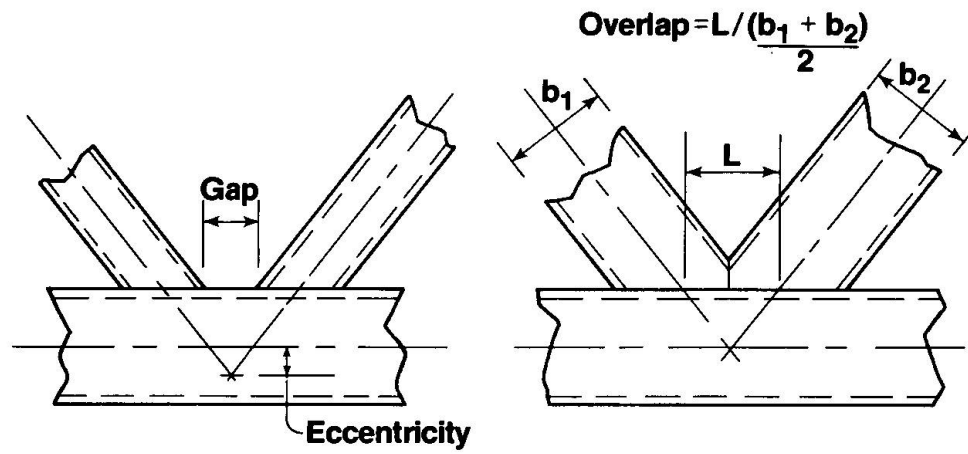12. Mang, F., and Striebel, A., Fatigue Strength Results, Internal Document, Universitat Karlsruhe, West Germany.

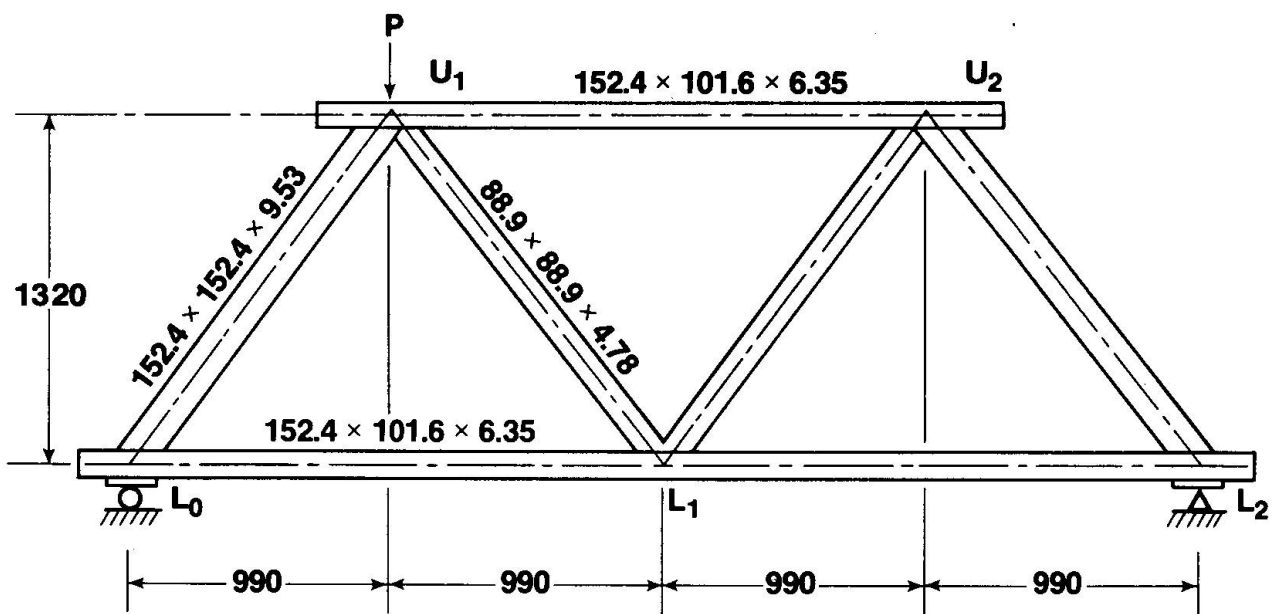Fig. 1   Gap and Overlap Type Joints
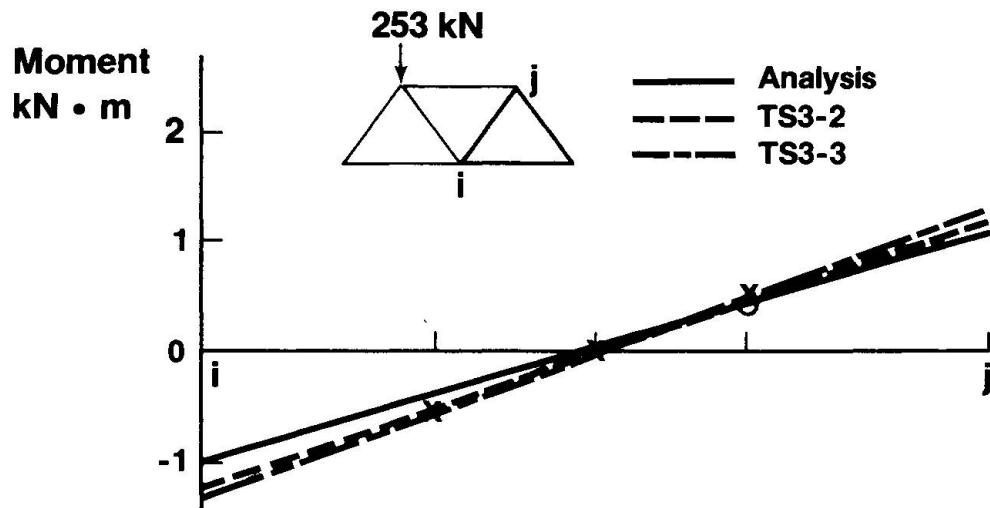

Fig. 2   Truss Configuration

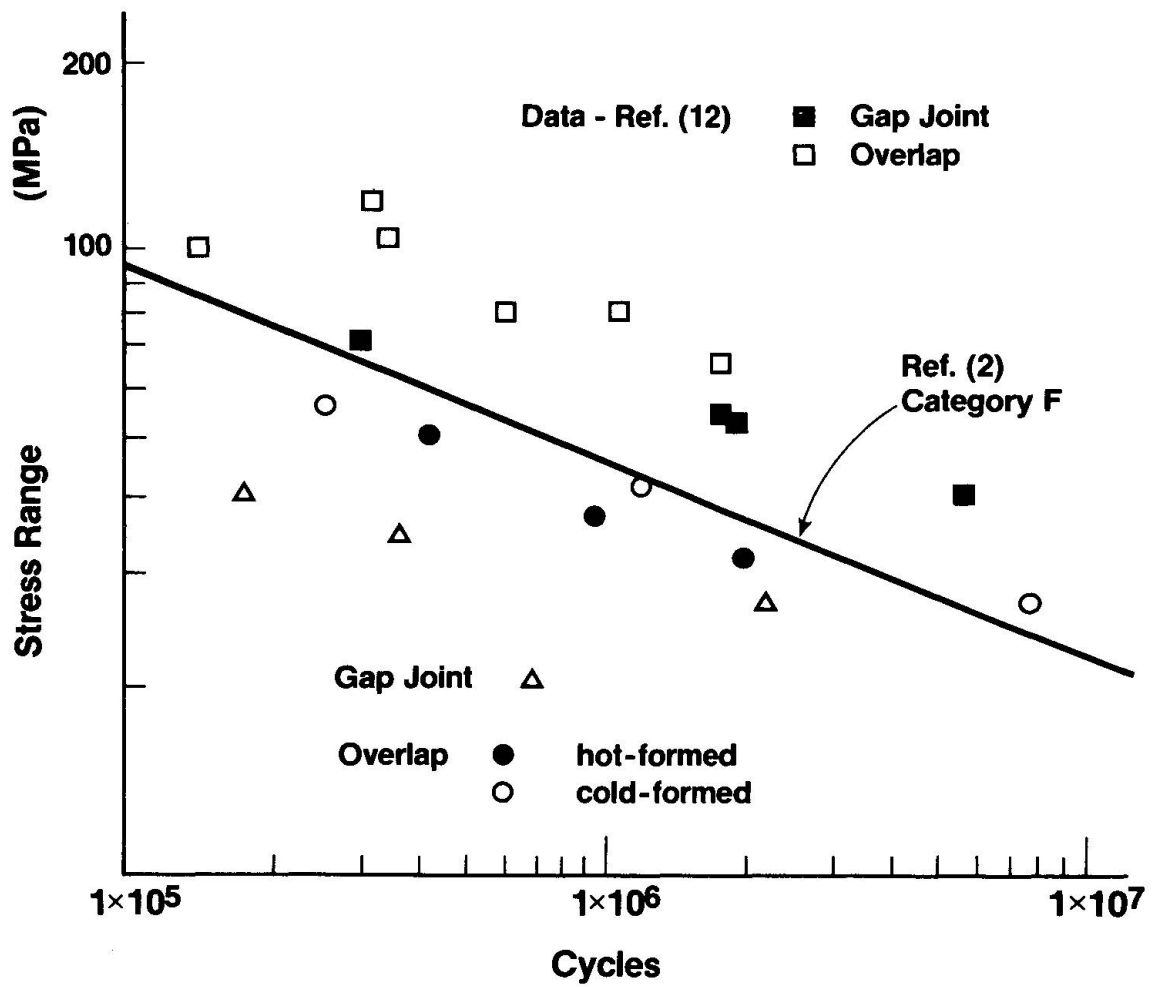Fig. 3   Measured and Predicted Bending Stresses

Fig. 4   Fatigue Strengths

Leere Seite

Blank page

Page vide

Design Considerations for Welded Hollow Section Joints

Remarques au sujet des assemblages soudés de profils creux

Bemessung geschweisster Verbindungen von Hohlprofilen

O.D. DIJKSTRA
IBBC-TNO
Rijswijk, the Netherlands

J. WARDENIER
Delft University
Delft, the Netherlands

C. NOORDHOEK
Delft University
Delft, the Netherlands

SUMMARY
After some general considerations in fatigue design, a review of the design curves for tubular joints is given. Curves for both nominal and hot spot stress ranges are shown. The method of determining the hot spot stress range is described. In addition, design curves for square hollow section joints are given. Finally, the fracture mechanics approach is outlined.

RESUME
Après quelques considérations générales sur le calcul à la fatigue on donne un aperçu des courbes de dimensionnement pour les assemblages de profils tubulaires. On montre les courbes pour les différences de contraintes aussi bien nominales qu'extrêmes. On décrit la méthode pour déterminer la différence de contraintes extrêmes. On donne en outre des courbes de dimensionnement pour les assemblages de profils creux à section carrée. Finalement, l'approche par la mécanique de rupture est esquissée.

ZUSAMMENFASSUNG
Nach einigen allgemeinen Betrachtungen über die Ermüdungsbemessung gibt der Beitrag eine Übersicht über die Bemessungskurven für Hohlprofilverbindungen. Es werden sowohl Kurven für nominelle als auch für extreme Spannungsdifferenzen vorgestellt. Die Methode zur Bestimmung extremer Spannungs-differenzen wird beschrieben. Zusätzlich werden Bemessungskurven für Verbindungen von Rechteck-rohren gegeben. Anschliessend wird die bruchmechanische Behandlung des Problems skizziert.

1. INTRODUCTION

Recently the results of an extensive ECSC research programme concerning the corrosion fatigue behaviour of steels in offshore structures have been reported [1]. Besides tests on welded flat steel specimens nearly 300 tubular joints were tested. The results of these tubular joint tests showed that the previously used AWS-X design curve was too optimistic for large sized joints. In the new editions of the AWS [2] and API [3] codes additional lower design curves are introduced for joints without an improved weld profile.
In the U.K. a draft for "New fatigue design rules" [4] ,based on the results of the European offshore research programme, has been published.
Last years also a by ECSC and Cidect funded research programme was carried out regarding the fatigue behaviour of joints in square hollow sections.
This paper reviews the existing design curves for joints in circular and rectangular hollow sections.

2. GENERAL CONSIDERATIONS IN FATIGUE DESIGN

For the determination of the fatigue life of a hollow section joint information is needed regarding:
- the loading in the members of the joint
- the S-N curve(s) to be used
- the stress distribution in the joint
- the influence of the environment
- a cumulative damage calculation procedure.

Generally the stress range S_r of the loading is taken into account whereas the stress ratio R is neglected, however for small sized joints it is shown that the influence of the R-ratio can be considerably [5,6]. The S_r-N curves can be given for the nominal stress range in the members or for the hot spot stress range in the joints. In the last method the S_r-N curves are generally valid but the stress distribution in the joint has to be known to calculate the maximum (hot spot) stress range. In both cases the stress ranges determined in design should be consistent with those used in the analysis of the test results (e.g. the determination of the stress concentration factors). Further the criterion of failure on which the S_r-N curves are based should be known (e.g. crack through the wall or complete failure).
Test in a corrosive environment (seawater) [1] have shown that the fatigue life of welded joints decreases by a factor of 2 to 3 and that no fatigue limit exists in the high cycle range.
For the calculation of the damaging effect of random loading the Palmgren-Miner rule is generally accepted. To prevent a fatigue failure (or a particular probability of failure) it is necessary to satisfy the condition.

$$\frac{n_1}{N_1} + \frac{n_2}{N_2} + \frac{n_3}{N_3} + \ldots\ldots\ldots\ldots = \Sigma \frac{n_i}{N_i} \leqslant D$$

where:
n_i is number of load cycles occuring with stress range S_i
N_i is number of load cycles, with stress range S_i, at which failure
       (or a certain probability of failure) occurs
D   is cummulative damage ratio being unity or smaller

3. FATIGUE DESIGN

3.1 General

In 3.2 and 3.3 the design curves taken from three codes are given. For a good comparison the following additional clauses in the codes have to be known.
- AWS-code [2]

   The curves are valid for redundant structures in atmospheric service. For critical members whose sole failure mode would be catastrophic, D shall be limited to a fractional value of 1/3.
- API-code [3]

   In general the design fatigue life of each joint and member should be twice the intended service life of the structure. For the design fatigue life, D should not exceed unity. For critical elements whose sole failure could be catastrophic, use of an additional margin of safety should be considered. The S_r-N curves are bases on an effective cathodic protection.
- DoE-code [4]

   The design S_r-N curves are based on the mean minus-two-standard-deviation curves for relevant experimental data. For a critical member, e.g. one whose sole failure would be catastrophic, an additional factor on life should be considered. For unprotected joints exposed to sea water the basic S_r-N curve is reduced by a factor of 2 on life. The basic S_r-N curve is given for 32 mm wall thickness. For wall thicknesses from 22 to 100 mm a correction on stress range has to be used being:

$$S_r = S_B \left(\frac{t_o}{t}\right)^{\frac{1}{4}}$$

Where:

t is the wall thickness of the detail under consideration

t_o is the wall thickness relevant to the basic S_r-N curve (wall thickness 32 mm)

S_B is the basic fatigue strength (wall thickness 32 mm)

S_r is the fatigue strength of the detail under consideration

For joints with wall thicknesses smaller than 22 mm no modification for the fatigue strength is given.

3.2 Nominal stress design curves for circular hollow section joints.

In fig. 1 the nominal stress design curves from the AWS- and API-code are given for circular hollow section joints. Table I shows the joints and stresses to which the curves apply. This together with the requirement that the design life has to be twice the service life according to the API, leads to a more conservative design using the API-code in stead of the AWS code. Use of the curves is simple, however it does not give a real impression of the safety because the curves are lower bounds for test results in the common range of application. Especially for relatively thick walled small sized joints these curves may be very conservative, whereas for large sized joints the thickness effect should be included. Better design procedures based on nominal stress and more consistent with those described in 3.3 are still in study.

3.3 Hot spot strain design curves

It is generally known that the fatigue strength of hollow section joints depends mainly on the hot spot stress- or strain range in a joint. The hot

spot stress-or strain range is the maximum stress-or strain range at the weld
toe and is influenced by: the global geometry of the joint, the global
geometry of the weld and the condition of the weld toe. In the various codes
and in the literature there are different definitions for the hot spot strain
range [7]. In the Working Group III of the European offshore research
programme the hot spot strain is defined as the extrapolated strain at the
weld toe through the strain measuring points A and B as shown in fig. 2. In
this way the influence of the geometry is included whereas the effect of the
weldtoe is excluded. This definition has also been adopted in the DoE-code
[4]. For geometries with pronounced three dimensional effects e.g. joints with
a diameter ratio of one, the distance between the measuring point B and the
weld toe should be 0.4 t. The stress-or strain concentration factor used in
design should be consistent with the definition used in the analysis of the
test results. Information regarding stress concentration factors can be found
in [8, 9 and 10] . In fig. 3 the hot spot strain design curves from the AWS-,
API- and DoE-code are given. The API-X, and AWS-X curves, are applicable for
the so called controled and improved weld profile. The same remarks as made
for the curves for nominal stresses are valid for the difference between the
API and AWS curves. The DoE-T line is steeper and has been based on the test
results of the ECSC programme and gives the mean minus-two-standard-deviation
curves for joints with wall thicknesses of 32 mm. As failure criterion is
taken crack through the wall which is roughly 80 % of the total life. For wall
thicknesses 22 < t < 100 mm the influence of the wall thickness is
incorporated by the function given in 3.1
For joints with wall thicknesses t < 22 mm no correction factors are given. An
analysis of the test results shows that for 4 < t < 22 mm the same correction
factor is applicable for $N = 10^7$ cycles, however the slope of the curves
change in such a way that the stress range at $N = 10^4$ remains nearly constant.

3.4 Classification method

For joints in rectangular hollow sections not sufficient information is
available for the determination of parametrical formulae for stress
concentration factors. Therefore S_r-N curves based on nominal stress range are
given but the main influencing geometrical parameters are taken into account.
The joints are classified in three basic types:
- K- and N-joints with gap
- K-joints with overlap
- N-joints with overlap
Within this classification and within the range of validity given (table II)
the wall thickness ratio is the main influencing parameter whereas the
influence of the other geometrical parameters is not significant.Fig. 4 shows
the S_r-N curves which are based on lower bounds minus two standard deviations
for each group. This figure shows the checking procedure for design which is
based on the nominal stress range in the members due to axial load and bending
moment. The connection between brace and chord is checked by using the curves
A, B or C respectively whereas the chord beside the joint is additonally
checked with curve D. The curves have been based on tests on joints with chord
dimensions up to 200 mm. For larger sections a preliminary scale function
(f(S)) is included which may be modified in future to bring it in line with
that for circular hollow section joints. The S_r-N curves given under 3.2 and
3.3 are safe for all R-ratios. It is shown however that especially for joints
with small wall thicknesses the R ratio can have a considerable influence.
This is the reason that these curves may only be used up to R = +0.2. For
higher R-ratios the S_r values have to be reduced. To prevent visual cracks
under serviceability condition a load factor of 1.2 is advised (about a factor
2 in life). More detailed information is given in [5, 6].

4. FRACTURE MECHANICS

The service life of welded connections with regard to fatigue can, in principle, be predicted with the aid of fracture mechanics. The governing parameter for fatigue is here the "stress intensity factor range" (ΔK).

$$\Delta K = f \ \Delta\sigma \ \sqrt{\pi a}$$

where: a = dimension of the defect (crack)
   Δσ = stress range
   f = geometric correction factor

The relation between ΔK and the crack growth is given in its simple form by the relationship of Paris and Erdogan:

$$da/dN = C \ \Delta K^m$$

where: da/dN = crack growth per cycle
   C and m are material constants, determined by simple fracture mechanics fatigue tests.

The service life can be calculated by:

$$N = \frac{1}{C} \int_{a_i}^{a_c} \Delta K^{-m} \cdot da$$

where: a_i = initial defect size
   a_c = critical defect size

ΔK can be determined by finite element calculations. For complex geometries, like tubular joints, these calculations are very difficult and time consuming. The disadvantage of fracture mechanics is the lack of experience with this approach. However, the advantages are a more general applicability and the possibility of calculating the remaining lifetime of a cracked node.

5. CONCLUSIONS AND REMARKS

Considering the fatigue behaviour of tubular joints shows that a design method based on hot spot stress is the most uniform design procedure. Comparison of the design curves of the existing codes with the test results shows that for joints with wall thicknesses t > 22 mm the DoE recommendations give the best approach. For joints with smaller wall thicknesses some modifications are possible to take the better fatigue performance into account however the approaches should be consistent for joints with t = 22 mm.
Information regarding stress concentration factors is available although this should be used with caution especially for complicated joints [4].
For joints in square hollow sections the classification method can be used although in future after obtaining more test evidence the methods given for circular- and square hollow section joints should be consistent with each other.
Although fracture mechanics provides a basis for understanding the importance of various parameters, at this stage not sufficient data is available to use this method in general.

REFERENCES

1. International Conference "Steel in Marine Structures" Paris, 5-8 October 1981
2. ANSI/AWS D1.1-81, American Welding Society, "Structural Welding Code", 1981.
3. API RP 2A, American Petroleum Institute, "Recommended Practice for Planning, Designing and Constructing Fixed Offshore Platforms", 1980.
4. United Kingdom Department of Energy, "Proposed New Fatige Design Procedures for Steel Welded Joints in Offshore Structures" June 1981 and Background to Proposed ..... Structures", May 1981.
5. Noordhoek, C., Wardenier, J and Dutta, D. "The fatigue behaviour of welded joints in square hollow sections". Part 2, Analysis. ECSC Convention 6210 KD-1-103 March 1980.
6. Wardenier, J. and Dutta, D. "The fatigue behaviour of lattice girder joints in square hollow sections" Conference "Joints in structural steelwork" Teeside, April 6-9, 1981/IIW document XV-493 / XIII-1005.
7. Dijkstra O.D., Back, J. de; "Fatigue strength of welded tubular T- and X-joints" OTC paper 3696, 1980.
8. Kuang, J.G., Potvin, A.B., and Leick, R.D.: "Stress concentration in tubular joints", OTC paper 2205, 1975.
9. Teyler, R. Gibstein, M. Bjorstad, H. and Haugan, G.: Parametrical stress analysis of T-joints" Technical report 77-253, Det Norske Veritas Oslo, November 1977.
10. Wordsworth, A.C. "Stress concentration factors at K- and KT-tubular Joints" Conference on Fatigue in Offshore Structural Steels, London, February 1981.

Table I   Nominal stress design curves for simple T, Y- or K connections.

type of weld	checked member	kinds of stress	design curves API	AWS
full penetration welds	brace	nominal brace stress range	D'	DT
partial penetration or fillet welds	brace	nominal brace stress range	E'	ET
controled/ improved profile	chord	punching shear stress range*	K	K_1
no controled/ improved profile	chord	punching shear stress range*	K'	K_2

* punching shear stress range V_p

$$V_p = \tau \sin\theta \left[\alpha \, f_a + \sqrt{(2/3 \, f_{by})^2 + (3/2 \, f_{bz})^2} \right]$$

τ = thickness ratio t/T
θ = brace angle
α = 1 for K connections; 2 for T- and Y-connections
f_a = axial load stress range
f_{by} = in-plane bending stress range
f_{bz} = out-of-plane bending stress range

Tabel II   Validity ranges of the various parameters

Parameter	
Θ_i	40° - 90°
b_i, h_i	$b_i = h_i$
b_o	≤ 450 mm
b_o/t_o	≤ 25
b_1, b_2	$b_1 = b_2$
$\beta = b_i/b_o$	0.5 ≤ β ≤ 1.0
$R = \dfrac{S_{r\,min}}{S_{r\,max}}$	- 1 ≤ R ≤ +0.2
Fe	Fe 360 Fe 510 St E 47 St E 70
gap	$0.5(b_o - b_i) \le gap \le 1.1(b_o - b_i)$
overlap	50% ≤ overlap ≤ 100%
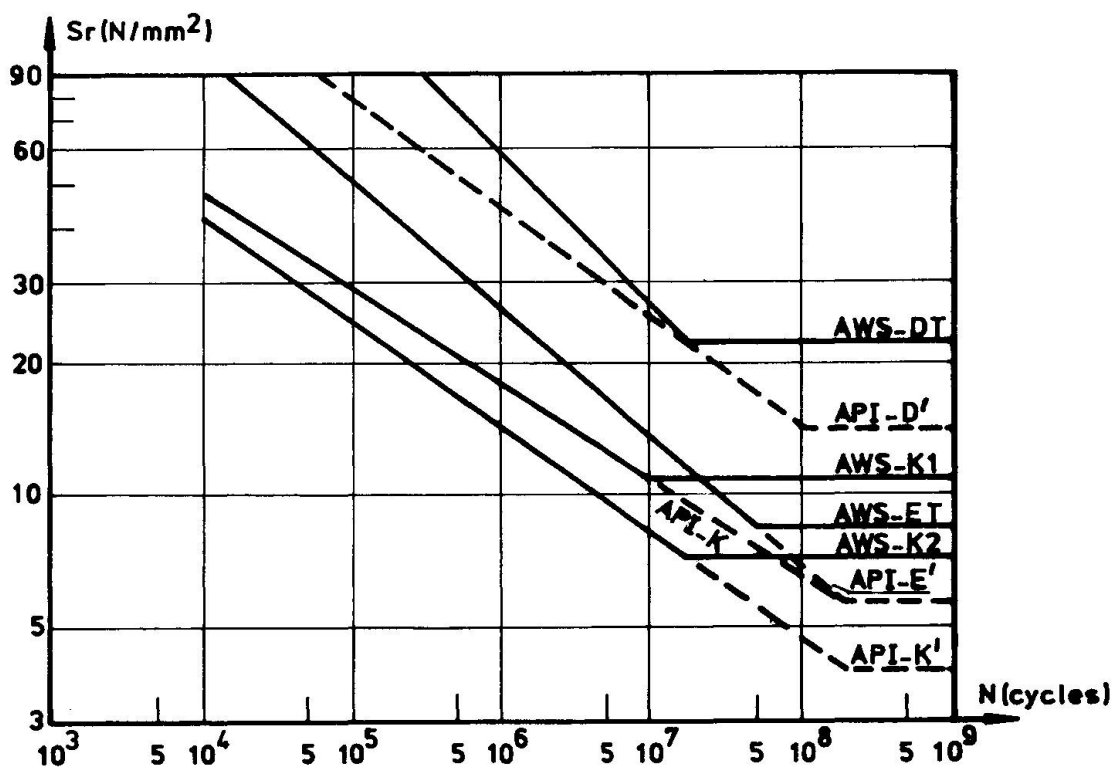
Fig. 1. Nominal stress curves taken from various design codes
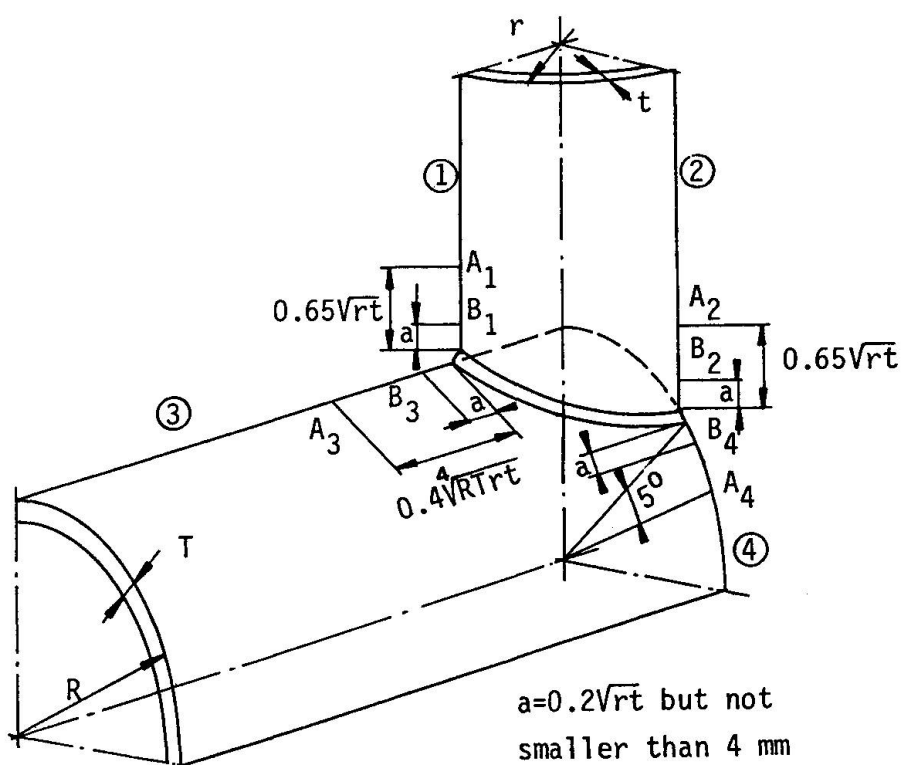

$a = 0.2\sqrt{rt}$ but not smaller than 4 mm

Fig. 2. Location of the points of the SNCF curve which has to be used for the extrapolation to the weld toe

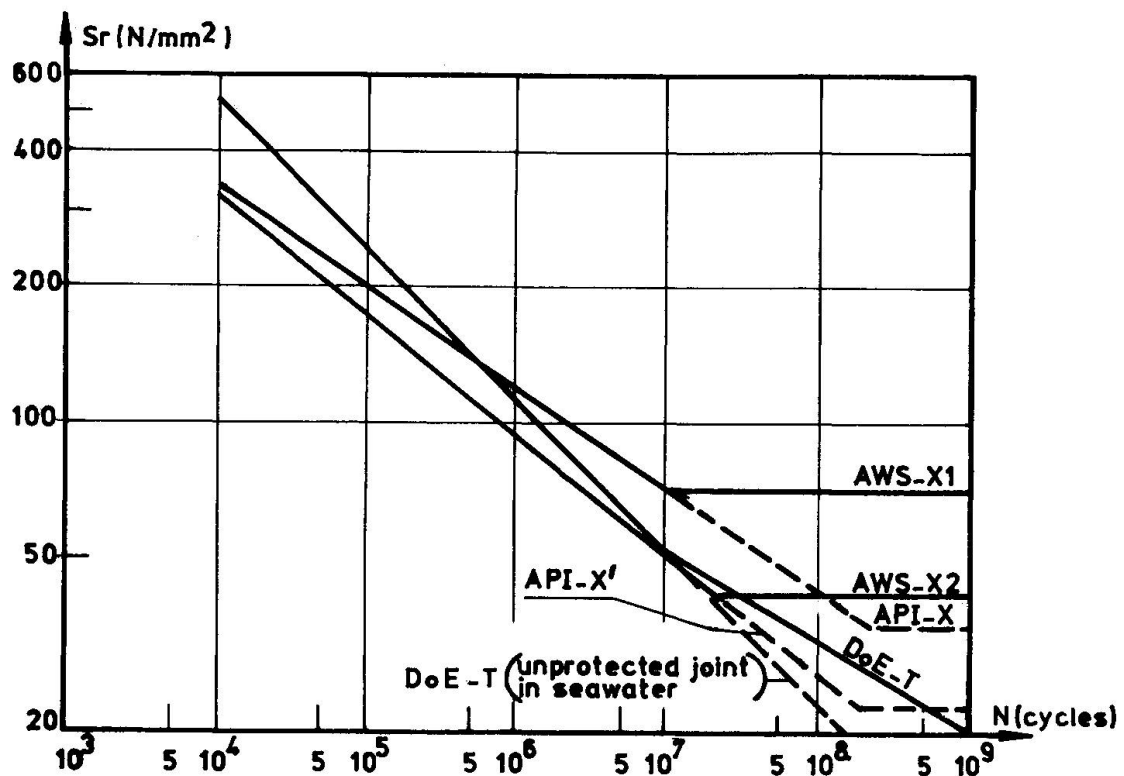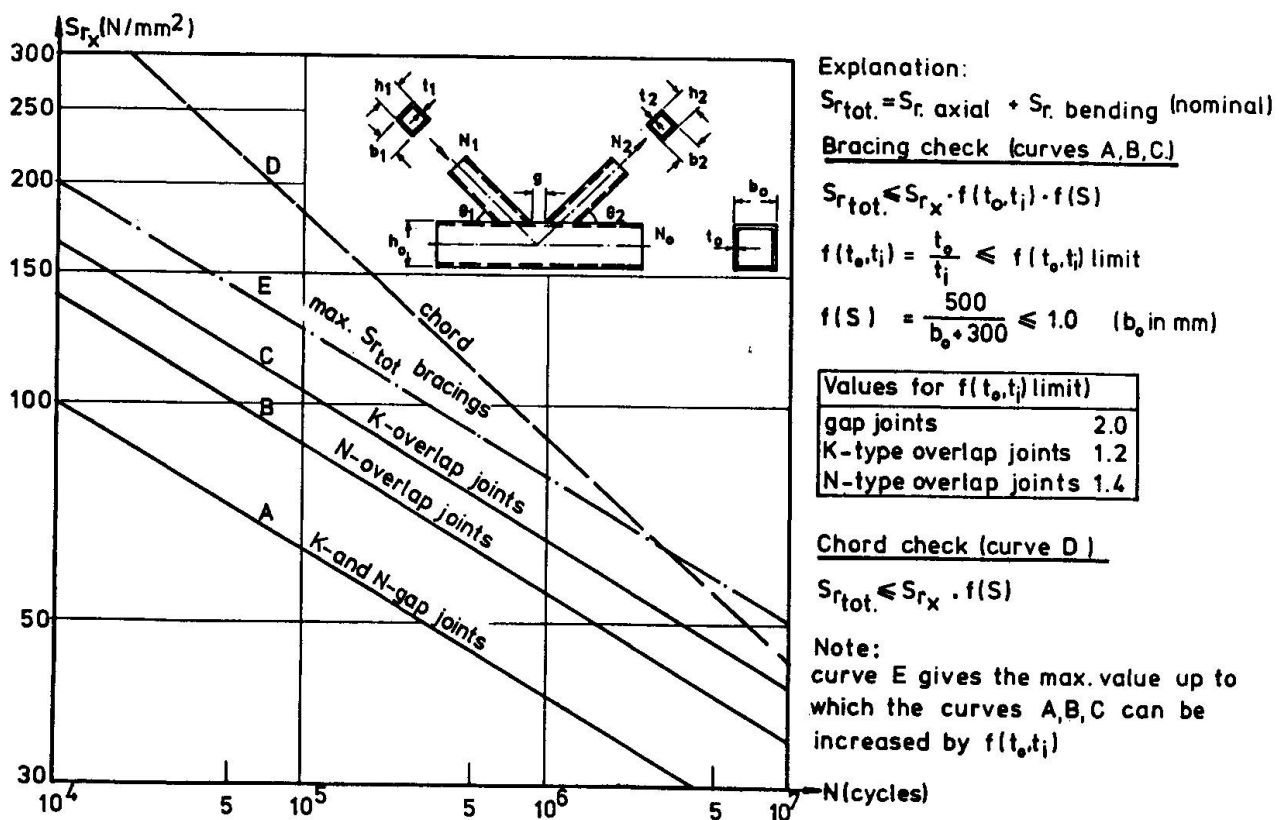Fig. 3. Hot spot stress curves taken from various design codes

Explanation:

$S_{r_{tot.}} = S_{r. \text{ axial}} + S_{r. \text{ bending}}$ (nominal)

Bracing check (curves A,B,C)

$S_{r_{tot.}} \leqslant S_{r_x} \cdot f(t_o, t_i) \cdot f(S)$

$f(t_o, t_i) = \dfrac{t_o}{t_i} \leqslant f(t_o, t_i)$ limit

$f(S) = \dfrac{500}{b_o + 300} \leqslant 1.0$ (b_o in mm)

Values for $f(t_o, t_i)$ limit)	
gap joints	2.0
K-type overlap joints	1.2
N-type overlap joints	1.4

Chord check (curve D)

$S_{r_{tot.}} \leqslant S_{r_x} \cdot f(S)$

Note:
curve E gives the max. value up to which the curves A,B,C can be increased by $f(t_o, t_i)$

Fig. 4 Recommended 95% survival S_r-N curves for K-and N-type joints made of square hollow sections

Fatigue of As-Welded and Stress Relieved Tubular T-Joints

Fatigue de branchements en T tubulaires soudés, recuits ou non

Ermüdung von unbehandelten und spannungsfrei geglühten, geschweissten T-Rohrverbindungen

C.D. SHINNERS
Engineer
Esso Australia
Sydney, Australia

A. ABEL
Associate Professor
The University of Sydney
Sydney, Australia

SUMMARY
As-welded and stress relieved large scale tubular T-joints were tested under static and dynamic loading. Strain distributions at the hot spots are presented and compared in relation to the specimen dimensions. Stress relieving was found to enhance fatigue performance with respect to both the cycles to crack initiation and failure. The complex crack propagation behaviour is also discussed.

RESUME
Des pièces de branchement en T tubulaires de grande dimension, en acier soudé, recuit ou non, ont été testées sous des charges statiques et dynamiques. Les distributions des déformations relatives aux endroits critiques sont montrées et sont comparées en relation avec les dimensions de l'échantillon. On a constaté qu'un recuit pour supprimer les contraintes résiduelles avait un effet favorable sur les caractéristiques de fatigue, aussi bien pour le nombre de cycles correspondant à l'apparition d'une fissure que pour celui correspondant à la rupture. Le comportement complexe durant la phase de propagation des fissures est également discuté.

ZUSAMMENFASSUNG
Geschweisste T-Verbindungen von Rohren mit grossen Abmessungen wurden unter statischer und dynamischer Belastung geprüft. Dies erfolgte sowohl mit unbehandelten als auch mit wärmebehandelten Prüfkörpern. Die Dehnungsverteilung an den gefährdeten Stellen wird aufgezeigt und in Verbindung mit den Dimensionen der Prüfkörper verglichen. Es hat sich gezeigt, dass die Wärmebehandlung das Ermüdungsverhalten verbessert und zwar im Stadium des Rissbeginns wie auch beim Ermüdungsbruch. Die komplexe Phase der Rissfortpflanzung wird ebenfalls behandelt.

1. INTRODUCTION

The deployment of welded tubular structures for the recovery of offshore crude
oil has lead to much needed research into the static and dynamic load behaviour
of the fatigue prone tubular joints. Such joints are susceptible to fatigue
simply as a welded joint but more importantly because of the coincidence of
regions of local stress concentration, known as hot spots, with the weld line.

Fatigue lives in air will largely be governed by hot spot strain magnitude and
the condition of welding. For this reason methods of estimating hot spot strains
in actual joints and theoretical models have been developed, and post weld pro-
cesses, for example grinding, have been investigated as possibilities for improv-
ing fatigue life. It is along these lines that three as-welded and two stress
relieved T-joints were statically and cyclically loaded to investigate the
influence of joint geometry on strain distributions and fatigue lives, as well
as the possible fatigue performance enhancement by stress relieving, known in the
case of small specimen welds.

2. EXPERIMENTAL DETAILS

2.1 Specimens

Five T-joint specimens were tested under axial brace loading as shown in Fig. 1.
This figure also shows the adopted convention for stress-strain dimensions. The
dimensions of the tubulars, as well as
the parameters typically used to define
joint geometry are given in Table 1.
On the basis of the test programme the
following five comparisons can be
made:

Specimens:

- 1 (as welded) and 2 (stress
                    relieved)

- 1 and 3 (thinner chord wall)

- 1 and 4 (smaller chord diameter)

- 4 (as welded) and 5 (stress
                    relieved)

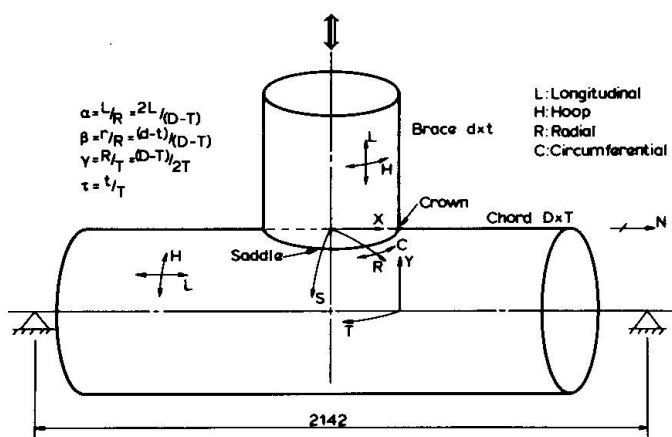-2 and 5 (smaller chord diameter)

$$\alpha = {^L/_R} = {^{2L}/_{(D-T)}}$$
$$\beta = {^r/_R} = {^{(d-t)}/_{(D-T)}}$$
$$\gamma = {^R/_T} = {^{(D-T)}/_{2T}}$$
$$\tau = {^t/_T}$$

Fig. 1 Specimen Configuration

Specimen	Condition	D	T	d	t	α	β	γ	τ
1	AW[1]	610	19.7	406	9.7	7.26	0.67	15.0	0.49
2	SR[2]	610	19.7	406	9.7	7.26	0.67	15.0	0.49
3	AW	610	12.3	406	9.7	7.17	0.66	24.3	0.79
4	AW	508	19.4	406	9.7	8.76	0.81	12.6	0.50
5	SR	508	19.4	406	9.7	8.76	0.81	12.6	0.50

(1) As Welded   (2) Stress Relieved

Table 1 Specimen Details

2.2 Materials, Welding and Post-Weld Heat Treatment

The seamed tubulars were rolled from steel designated AB3603, according to Australian Iron and Steel Company terminology, developed for offshore platforms in Bass Strait, Australia. Tensile properties of the steel are provided in Table 2.

	Yield Strength MPa	Ult. Strength MPa	% Reduction of area	% Elongation in $5.65\sqrt{S_0}$
Specified	250 Min	410 Min	-	22 Min
Measured (1)	244,244[3]	382	76	40
(2)	244,340	458	58	34

(1) Tube longitudinal direction.

(2) Tube circumferential direction after flattening of tube.

(3) Second value represents 0.2% proof stress

Table 2   Tensile Properties of AB3603

A manual-metal-arc welding method was used by the fabricators with experience in the offshore industry. Welding preparation and procedures were according to AWS Structural Welding Code D1.1-72 with the exception that a single weld run was deposited from inside the brace.

The following post-weld heat treatment procedure was used in the case of specimens 2 and 5: heating at 100°C/hr, hold for 1 hour between 580 and 620°C, cooling at 150°C/hr to 300°C, followed by air cooling.

2.3 Strain Gauging and Instrumentation

All specimens were strain gauged around the weld line on both the brace and chord inside and outside surfaces. At the saddle positions gauges were attached radiating from the weld toe on the chord side to enable determination of hot spot stresses and strains by extrapolation. Combinations of rosette gauges, strain gradient gauges and single element gauges were used. The rosettes were necessary for determining stress distributions in the biaxial stress fields existing around the weld line. Symmetrical gauges, specifically higher up the brace, permitted a check of specimen alignment and axiality of loading. Specimen 1 was also monitored with a large number of rosettes attached away from the weld line in order to improve on the gauge positioning for the subsequently tested specimens.

2.4 Crack Growth Monitoring

Crack initiation was detected through monitoring of strain behaviour adjacent to the weld toe at the hot spots. Visual observation and confirmation of the crack was aided by a low power magnifying glass and a highly volatile solvent which, when applied to the specimen surface under dynamic loading, bubbled in the vicinity of a crack. The same technique was used for surface crack growth measurements.

Crack marking provided information about through thickness crack growth in specimens 2 to 5 and ultrasonic techniques were tried in the case of specimens 1 and 2. In specimens 2 to 5 a combination of appropriately placed "sacrificial" strain gauges and specially developed crack propagation gauges were used. A constant current was applied to the gauges consisting of a parallel multi wired

arrangement so that a wire breaking was detected by a change in voltage across
the gauge.

2.5 Experimental Procedure

Initially each specimen was subjected to two incremental static load cycles,
between which, specimen alignment was adjusted and hot spot strain amplitudes
were checked. This was followed by fully reversed (R = -1) sinusoidal dynamic
loading which was interrupted periodically to monitor all strain gauges under
static loading.

The load amplitudes, directed towards high cycle fatigues were selected to achieve
the same hot spot strain amplitude for each specimen.

3. STATIC RESULTS

3.1 Strain Distributions

Figure 2 shows the radial strain distribution along the chord S-axis for specimens
1, 3 and 4. In plotting only one side, symmetrical gauges have been averaged.
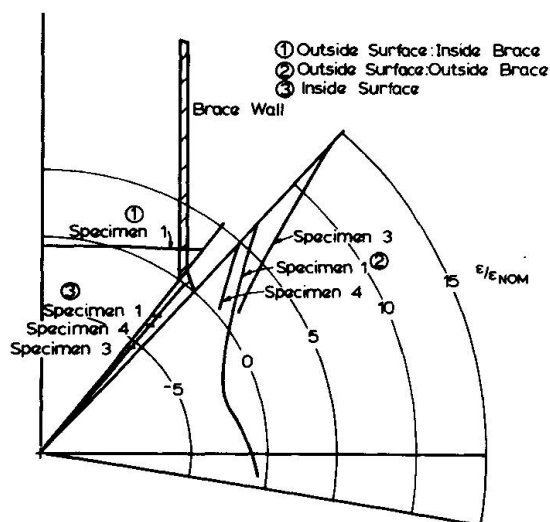

The distributions have been plotted as
the ratio of measured strains to the
nominal brace membrane strain, ε_{NOM}, for
each specimen. This is calculated from
ε_{NOM} = (P/Ab)/E where P is the axial
load and Ab is the cross-sectional area
of the brace wall.

For the joint and loading configuration
investigated, the normalised strains
typically correspond to the maximum
principal strains, the principal stress
direction on the chord surface being
radial to the brace. This is not the
case within the restraining brace where
the maximum strains, at the top centre
of the chord, correspond closely to the
(maximum) nominal bending strains and
hence are aligned in the longitudinal
direction. Figure 2 clearly shows the
existence of the hot spot or area of
stress concentration at the saddle weld
toe. The effect of a reduction in chord

Fig. 2   Radial Strain Distribution
         in Chord along S-axis:
         Specimens 1, 3 and 4

wall thickness is seen to produce a much steeper strain gradient approaching the
weld toe and, comparing inside and outside surface strains, a higher contribution
of membrane strain. A reduction in chord diameter has done little to the strain
gradient and simply produced an overall reduction in strain concentration. The
contribution of membrane strains is seen to be very low.

3.2 Stress-Strain Concentration

The ratio of hot spot strains to the nominal brace strains can be seen to be high-
est for specimen 3 and lowest for specimen 4. Normally the hot spot stresses/
strains used to calculate stress-strain concentration factors (SCF's/SNCF's) are
those existing at the weld toe but not influenced by local weld geometry or
microscopic defects such as pits or cracks. In tubular joint specimens they have
been determined either by linear extrapolation from two gauge readings [e.g. 1]
or curved extrapolation from a number of readings [e.g. 2] taken radially to the

intersection line. Curve fitting in this case is generally done by eye. Linear extrapolation was proposed as a means of reducing the subjectivity involved with curve fitting in a region of such steep strain gradient. The recommended gauge locations for linear extrapolation have varied in the past but typically have been defined by a distance from the weld toe given by some function of $\sqrt{RT}$ or $\sqrt{rt}$ for the brace or chord respectively. To avoid weld toe influences a minimum distance to the closest gauge was originally set at 4 mm [3], although more recently 0.4T was concluded to be the limit of influence [4].

In Table 3, SCF's and SNCF's are given for the brace and chord saddle of specimen 4 as well as actual and recommended reading points for linear extrapolation. This Table shows the effect of linear extrapolation in significantly reducing

	CHORD		BRACE	
	SCF/SNCF	Extrapolation points	SCF/SNCF	Extrapolation points

SCF   Curve
      Linear 1
      Linear 2
	5.8
	5.2
	5.4
		0.4T,0.2√RT + 5°
		0.4T, 5°
			4.6	0.2√rt,1.4√rt

SNCF   Curve
      Linear 1
      Linear 2
	4.7
	4.2
	4.4
		0.4T,0.2√RT + 5°
		0.4T, 5°
			4.9
			3.7
			4.1
				0.2√rt,1.4√rt
				0.2√rt,0.65√rt

Recommended (2) (5&6)		(1)0.2√RT,0.2√RT + 5° 0.4T, 5°		0.2√rt,0.65√rt 0.2√rt,0.65√rt
Predicted SCF Wordsworth (7) Kuang(3) (8) Teyler (9)	5.1,4.9(2) 3.6 4.0		4.2,4.1(2) 4.8 5.0	

(1) Minimum set at 4 mm
(2) Corrected for weld leg length
(3) $\beta = 0.81$, Formulae valid $\beta < 0.8$

Table 3   SCF's/SNCF's for Specimen 4:   Saddle Position

estimated SCF's and SNCF's in both the brace and chord. The difference between the linearly extrapolated values is not high but this would be influenced by the fact that the same "closest" reading was used in each case, namely that at 0.4T. If the previously recommended 0.2√RT had been used in the case of the chord, as was done for the brace, then the corresponding values for the SCF and SNCF would have been even lower.

A comparison with the predictions for the SCF's from the formulae of Wordsworth and Smedley [6], Kuang et al. [7] and Teyler et al. [8] is also given in Table 3. For this specimen, the "uncorrected" formulae of Wordsworth and Smedley, obtained from acrylic model studies, is seen to provide the most accurate prediction for the chord SCF. The formulae of Teyler et al., obtained from curved thin shell finite element studies, agree best with the brace SCF. It should be noted however that the brace SCF was obtained only from linear extrapolation and therefore would be lower than the "actual" SCF. The chord SCF obtained by curved extrapolation in specimen 5 was 5.0, as opposed to 5.8 for specimen 4, and this former value agrees very well with the prediction of Wordsworth and Smedley.

4. DYNAMIC RESULTS

4.1 Influence of Stress Relieving

As described above, crack initiation was detected using both strain monitoring and visual observation. Failure was defined by a rapid increase in joint deflection. Table 4 provides the fatigue results of all specimens in terms of the number of cycles to crack initiation and failure as functions of the hot spot strain ranges. These were determined using full extrapolation to the weld toe of strain measurements under both tensile and compressive loading, and then summing the two. Data is provided for both the east and west sides for each joint

Specimen	$\Delta\varepsilon_{Hot\ Spot}$		East		West		N_f
	E	W	$Nc^{(1)}$	$Nc^{(2)}$	$Nc^{(1)}$	$Nc^{(2)}$	$\times 10^6$
1	777	820	$0.332^{(3)}$	0.1	$0.32^{(3)}$	0.1	2.55
2	738	835					20
2	1494	1645	0.1	0.05	0.05	0.04	0.6
3	793	765	0.45	$0.4^{(4)}$	0.45	0.5	1.55
4	738	789	0.087	0.05	0.056	0.04	0.941
5	685	690	3.25	2.5	3.8	5.0	9.07

(1) Visual observation

(2) Strain drop at hot spot under tensile load

(3) Crack length > 80 mm, i.e. initiation missed

(4) Strain redistribution as crack initiation site not coincident with strain gauge

Table 4   Fatigue Data for all Specimens

As can be seen from the Table, specimen 2 did not show any signs of fatigue damage after 20 million load cycles. At this stage cycling was recommenced at twice the load amplitude. A comparison of specimens 1 and 2, and 4 and 5 indicates the beneficial effect of stress relieving in terms of improvement in both cycles to crack initiation and cycles to failure.

The thin walled specimen 3 showed a superior life to crack initiation. This is probably in line with the dimensional influence on fatigue strength observed elsewhere [9]. The fact that the fatigue life was not superior to that of the other specimens suggests that it was not necessarily a simple thickness effect but differences in residual stress states may also be involved.

Using the strain indicated crack initiation data, and the hot spot strain data for the joint side to indicate first cracking, the results of Table 4 have been plotted in Fig. 3 to further s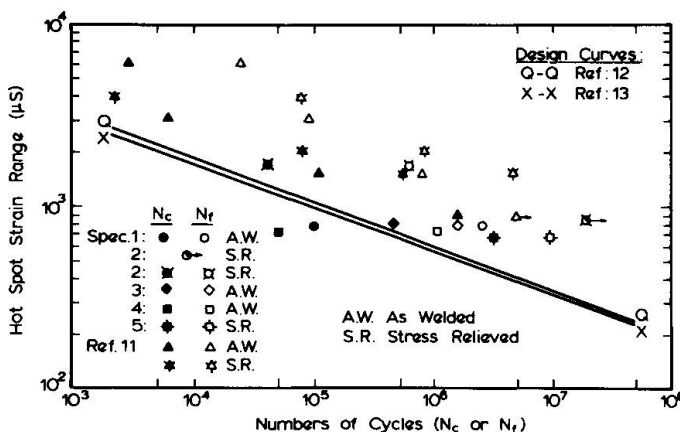how the influence of the stress relieving. Also shown in Fig. 3 is the as-welded and stress relieved fatigue data of Yamaski et al. [11] who concluded that stress relieving had no influence on fatigue strength. Although statistically not sifgnificant two of their specimens tested at the same load range clearly show a superior fatigue strength for the stress relieved specimen. One futher remark about the cited work is that most of the specimens were tested at higher strain ranges at which the influence of residual stresses will be reduced.

Two appropriate tubular joint design curves, from the Department of Energy [Q-Q curve, Ref. 12] and the American

Fig. 3   Comparison of As Welded and Stress Relieved Fatigue Data

Petroleum Institute (X-X curve, Ref. 13), drawn on Fig. 3 indicate conservatism
with regard to failure for these specimens but not in terms of crack initiation.

4.2 Crack Propagation

In all specimens crack initiation occurred in the vicinity of the hot spots of
the chord side weld toe. Crack propagation continued simultaneously around the
weld toe and into the chord wall. Loss of joint rigidity typically occurred
when the surface cracks were approaching the crowns. Figure 4 shows the surface
crack propagation in the as-welded
specimen 1. This figure illustrates
fairly symmetrical and uniform crack
growth rates resulting from stress
redistribution away from the higher
stressed saddle towards the lower
stressed crown [14]. Figure 4 also
indicates crack branching on the east
side, whereby secondary cracks propag-
ated away from the chord wall towards
the direction of the chord longitudinal
axis. Crack growth rates for these
secondary cracks can be seen to be
significantly lower than for the weld
toe crack.

Fig. 4   Specimen 1:   Crack Growth in
         Millions of Cycles

The crack path through the chord wall
in specimen 1 is shown for the west saddle and near the north crown in Fig. 5.
At the saddle four distinct stages of propagation can be identified following
initiation at the weld toe. Stage 1 growth was normal to the chord surface and
continued to a depth of about 2-3 mm to the limit of the heat affected zone.
This type of growth extended the full
length of the crack and the surface
was generally smooth and flat. At the
saddle the growth then changed direc-
tion to being normal to the brace axis,
stage 2. This indicates a triaxial
stress state with maximum stresses
arising directly from the brace-chord
load transfer rather than the resulting
chord wall bending. The surface of
this stage of growth was irregular and
indicative of a combination of opening
mode I and shear mode II type crack
growths [15]. Mode II type growth
tends to bring out the structural
feature of the parent material. The
third stage of growth, stage 3, was
normal to the chord wall again and
left a smooth surface. Increased

Fig. 5   Specimen 1:   Through Wall Crack
         Paths

bending stresses from the reduced wall thickness would have changed the crack
growth direction. Eventually the remaining ligament was so small through
cracking occurred with the formation of a shear lip, stage 4. Away from the
saddles stage 2 growth was not evident and so chord wall bending (and membrane)
stresses must have continually dominated. The above serves to illustrate the
complex fatigue behaviour of tubular joints and the difficulty in applying
techniques such as fracture mechanics to life prediction.

5. CONCLUSIONS

For large scale tubular T-joints subjected to static and dynamic axial brace loading,

- reduction of chord wall thickness significantly increased radial strain gradients at the saddle hot spots whilst reducing the chord diameter simply reduced the strain magnitudes without significantly affecting strain gradients,

- linear extrapolation techniques estimate stress and strain concentration factors that are significantly lower than those determined from curve fitting to more than two readings,

- stress relieving significantly improves the fatigue strength with regard to crack initiation and final failure, and

- through wall crack propagation paths varied around the weld toe circumference depending upon the developing stress states.

REFERENCES

1   DIJSTRA, O.D., de BACK, J.: Fatigue Strength of Tubular T- and X-Joints. Paper No. OTC3696, 12th Annual Offshore Technology Conf., Texas, May, 1980.
2   NOEL, J.S., BEALE, L.A., TOPRAC, A.A.: An Investigation of Stresses in Welded T-Joints. Report No. S.F.R.L. Tech. Rept. p. 550-3, Structures Fatigue Res. Lab., Dept. of Civil Engineering, The Univ. of Texas, 1963.
3   De BACK, J.: Report on Session 10, Testing of Tubular Joints. European Offshore Steels Select. Seminar, Cambridge, 1978.
4   WARDENIER, J.: Private Communication, May 1981.
5   WARDENIER, J.: Some New Developments in the Design of Large Metal Structures. Keynote Address: Metal Structures Conference, 1981, Newcastle (Aust.), Inst. of Engrs Aust., May, 1981.
6   WORDSWORTH, A.C., SMEDLEY, G.P.: Stress Concentrations at Unstiffened Tubular Columns. European Offshore Steel Select. Seminar, Cambridge, 1978.
7   KUANG, J.G., POLVIN, A.B., LEICK, R.D.: Stress Concentration in Tubular Joints. Paper OTC2205, 7th Annual Offshore Technology Conf., Texas, May, 1975.
8   TEYLOR, R., GILSZTEIN, M., BJØRNSTAD, H., HAUGAN, G.: Parametrical Stress Analysis of T-Joints. Det Norske Veritas, Report No. 77-523, November, 1977.
9   WYLDE, J.G., McDONALD, A.: The Influence of Joint Dimensions on the Fatigue Strength of Welded Tubular Joints. Int. J. Fatigue, Jan. 1980.
10 GURNEY, T.R.: Fatigue of Welded Structures. Snd Ed. Cambridge Univ. Press, Cambridge, 1979, Chap. 10.
11 YAMASAKI, T., TAKIZAWA, S., KOMATSU, M.: Static and Fatigue Tests on Large-Size Tubular T-Joints. Paper OTC3424, 11th Annual Offshore Technology Conf., Houston, Texas, May, 1979.
12 DEPARTMENT OF ENERGY: Offshore Installations: Guidance on Design and Construction. London, July, 1977.
13 AMERICAN PETROLEUM INSTITUTE: Recommended Practice for Planning, Designing and Constructing Fixed Offshore Platforms, APO RP2A, 11th Ed., Jan. 1980.
14 SHINNERS, C.D., ABEL, A.: Stress Analysis of Large Scale Tubular T-Joints. Symposium on Stress Analysis for Mechanical Design, 1981. The Institution of Engineers, Australia, National Conf. Publication No. 81/4.
15 DOVER, W.D., HOLDBROOK, S.J.: Fatigue Crack Growth in Tubular Welded Connections. Int. J. Fatigue, Jan. 1980.

Fatigue Characteristics of Steel Plate Decks for Steel Bridges

Caractéristiques de fatigue des tabliers métalliques pour les ponts en acier

Ermüdungseigenschaften von Stahlfahrbahnplatten für Stahlbrücken

YUKIO MAEDA
Prof. Dr. -Eng.
Osaka University
Suita, Osaka, Japan

MASANORI SERA
Master of Eng.
Osaka University
Suita, Osaka, Japan

SUMMARY
This paper presents the results and a discussion of full scale model tests to study the initiation and propagation of fatigue cracks in steel plate bridge decks. The observed fatigue cracks are then classified according to pattern and stress condition. Factors affecting fatigue crack initiation are identified by detailed examination of the stress conditions. Finally the reduction of fatigue strength in the welded deck joints is discussed in relation to weld defects.

RESUME
Cet article présente les résultats et une discussion d'essais sur modèle en grandeur nature pour étudier l'initiation et la propagation de fissures dues à la fatigue dans les tabliers métalliques de pont. Les fissures observées, dues à la fatigue, sont classées selon leur type et leur condition de contraintes. Les facteurs affectant l'initiation d'une fissure de fatigue sont identifiés par l'examen détaillé des conditions de contrainte. Finalement la résistance à la fatigue dans les joints soudés du tablier est discutée en relation avec des défauts de soudure.

ZUSAMMENFASSUNG
Der Beitrag stellt die Ergebnisse von Versuchen an Fahrbahnplatten aus Stahl vor. Die Versuche hatten das Studium des Rissbeginns und der Rissfortpflanzung zum Ziel. Die beobachteten Ermüdungsrisse sind gemäss ihrem Typ und dem zugehörigen Spannungszustand klassiert. Aufgrund einer detaillierten Untersuchung des Spannungszustandes werden Faktoren, die den Rissbeginn beeinflussen, identifiziert. Schliesslich wird die Reduktion der Ermüdungsfestigkeit geschweisster Verbindungen in Fahrbahnplatten im Zusammenhang mit Schweissfehlern diskutiert.

1. INTRODUCTION

A steel plate deck for a steel bridge consisting of longitudinal ribs, transverse floor beams and a deck plate, is an assembled welded structure subjected directly to repeated vehicle loads. The fact that fine fatigue cracks were found out in the longitudinal stiffeners below the deck plate of some of existing bridge, was reported [1]. Therefore, it is necessary to study on the fatigue behavior of the steel deck. Fatigue strengths of some models of welded joints to be used at the deck have been obtained for small coupon-type specimens under repeated axial tensile stresses. In practical problems, however, each element of such a structure will be in complicated stress conditions.

To study on the initiation and propagation of fatigue cracks of steel plate decks, the authors have been carrying out fatigue tests of their full-sized models such as orthotropic decks with open-shaped longitudinal ribs and hollow decks with V-shaped longitudinal ribs. The fatigue test results of the orthotropic deck panels were reported [2]. It was also reported that the hollow deck tested had the great fatigue strength because of no observation of fatigue crackings [3]. Furthermore, for a hollow deck panel with a smaller thickness than that of such a test deck as mentioned above, a fatigue test was conducted, assuming that the traffic direction was perpendicular to the V-shaped longitudinal ribs.

In this paper, the fatigue test results of the orthotropic deck panels and the hollow deck panel with a smaller thickness are presented and discussed. The observed fatigue cracks could be classified into several patterns in accordance with the stress condition. Then, the authors will discuss the pattern of fatigue cracks in combination with stress analysis around the cracks by the finite element method.

2. OUTLINE OF TESTS

2.1 Test Panels

Test panels are two kinds of orthotropic decks with open-shaped longitudinal ribs as shown in Fig. 1 and a hollow deck with V-shaped longitudinal ribs as shown in Fig. 2.

Details of the test panels are given as follows:
(a) The steel material is structural steel of SS41 designated at the Japanese Industrial Standards (JIS). Mechanical properties of the plates
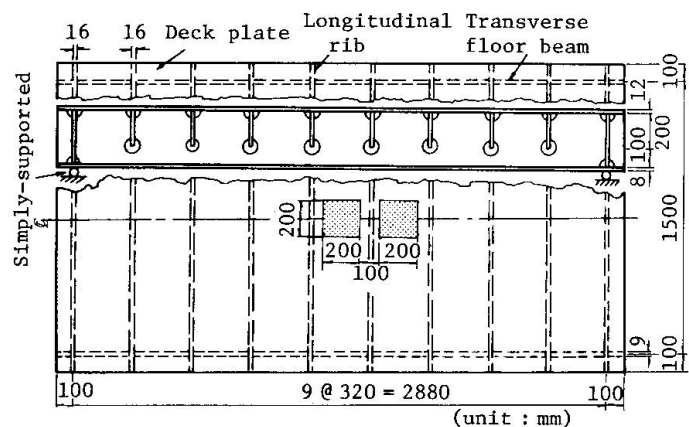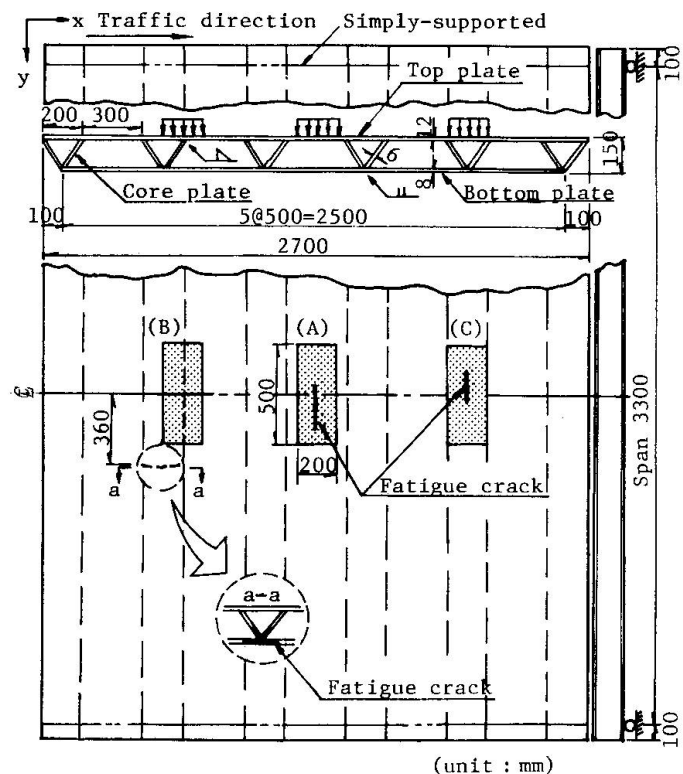

Fig. 1 Orthotropic deck panel

Fig. 2 Hollow deck panel

of all of the panels are given in Table 1.
(b) The longitudinal ribs of the orthotropic deck
panel were welded to the floor beam webs on the
both sides or one side only as shown in Fig. 3.
The former is called Type-1 joint and the latter
Type-2 joint. The panel as shown in Fig. 5(a) has
Type-1 joints in two floor beams and the panel as
shown in Fig. 5(b) has Type-1 joints in a floor
beam and Type-2 joints in another one.
(c) Fabrication process for the hollow steel deck
is shown in Fig. 4. At first, core plates forming
evenly-spaced triangles were welded to the top
plate by fillet welding. Next, the bottom plates
were welded strip by strip to the core plates by
butt welding.

2.2 Test Procedures

All panels have two opposite simply-supported
edges and two free edges. The supported line is
indicated in Figs. 1 and 2.

A load is applied at the locations as shown in Figs.
1 and 2 by a hydraulic jack of a Losenhausen type
fatigue testing machine.
A size of loading pads was
determined by considering
rear double tires of a
design truck. Firstly, each
panel was loaded statically
in order to investigate the
elastic behavior of the
test panel. Then, a dynamic
repeated load was applied
to the panel at the rate of
about 5 Hz.

During the fatigue test, a
repeated loading was inter-
rupted to measure deflec-
tions and strains at vari-
ous points. Since it was
difficult to find out
fatigue cracks visually,
two inspection methods were
used together to determine
the fatigue life. One was
a liquid penetrant inspec-
tion and the other was an
estimation method of pick-
ing up changing points of
dynamic strin range histo-
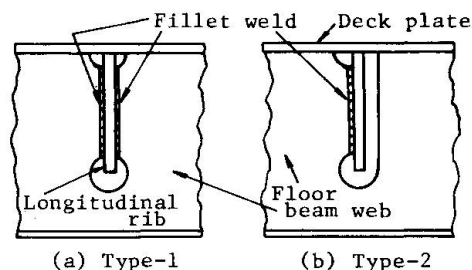ries at the points where
crack initiation was
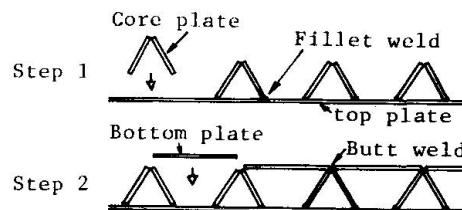expected.

Fig. 3 Details of inter-
section

Fig. 4 Fabrication of
hollow deck

Table 1. Mechanical properties of plates

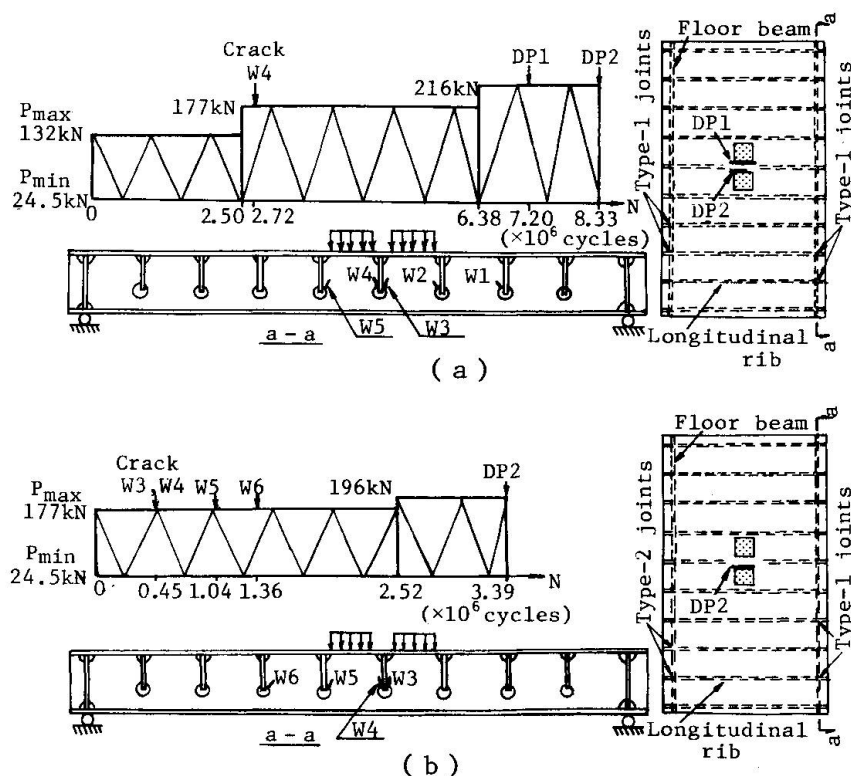| Specimens	Yielding point σ_y (MPa)	Tensile strength σ_t (MPa)	Elongation (%)	Young's modulus E_s (GPa)
SO	311	445	27.6	196
SV	278	419	28.7	201
JIS-SS41	$\geq$245	402 - 510	$\geq$17.0	—

(a)

(b)

Fig. 5 Testing records and locations of cracks

2.3 Test Results

2.3.1 Orthotropic Deck Panel

Fatigue testing records and locations of fatigue cracks are shown in Figs. 5(a) and (b). In the both panels, the first crack 'W4' occurred at the intersection of a longitudinal rib and a floor beam web. Next, the fatigue cracks 'W2' and 'W5' were observed during the fatigue test.

All of the fatigue cracks in the floor beam web were initiated at the fillet weld toes at the upper part of circular cutouts in the web. The fatigue cracks 'W3' and 'W4' propagated upward along the fillet weld toe. The fatigue cracks 'W5' and 'W6' developed toward the center of loading in the floor beam web as shown in Fig. 6. At the final stage, a fatigue crack 'DP1' occurred in the deck plate between loads as shown in Fig. 5(a).
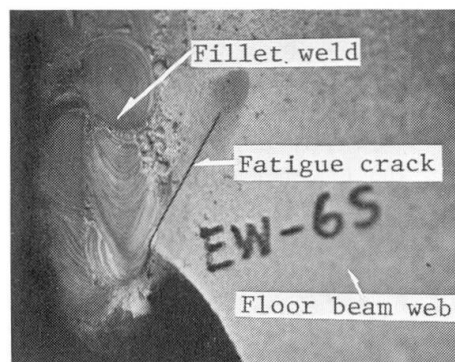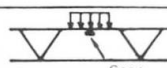

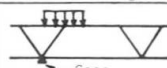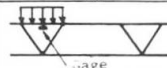Fig. 6   Fatigue crack in floor beam web
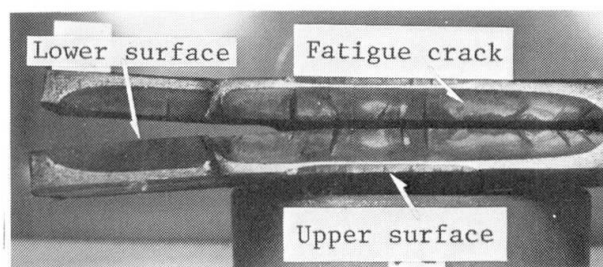
Fig. 7   Fracture surface of top plate

2.3.2 Hollow Deck Panel

Fatigue tests were conducted for three loading cases which could be considered as independent each other. Loadings at the fatigue tests are summarized in Table 2. The locations of the fatigue cracks are indicated in Fig. 2. Fatigue cracks at the loading cases A and C were initiated at a top plate below a loading pad. A typical fracture surface of these cracks is shown in Fig. 7. A fatigue crack at the loading case B was initiated at a longitudinal butt welded joint at which core plates were connected to a bottom plate. The fatigue crack propagated into both the bottom and core plates perpendicular to the longitudinal butt weld line. The fracture surface of this crack is shown in Fig. 8.

Table 2.   Testing records of hollow deck panel

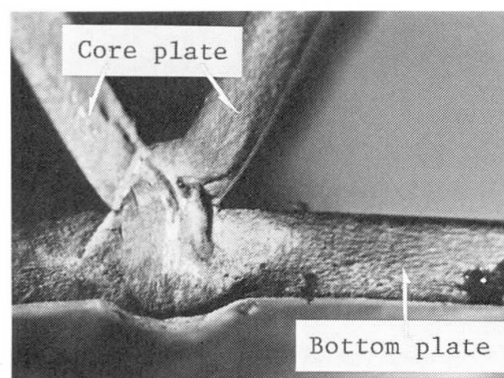| Loading conditions		Load (kN)		No. of cycles ($\times 10^6$)	Stress range (MPa)
		P_{max}	P_{min}		
A		147	19.6	0 - 3.00	212
		235	19.6	3.00 - 3.42	297
B		177	19.6	0 - 3.00	82
		245	19.6	3.00 - 4.01	117
C		147	19.6	0 - 3.00	210
		196	19.6	3.00 - 3.65	278

Fig. 8   Fracture surface of butt weld

3. FATIGUE BEHAVIOR

3.1 Pattern of Fatigue Cracks and Stress Conditions

Fatigue cracks observed at the tests are classified into the following patterns:
(a) Cracks in base metals such as a deck plate and a top plate,
(b) Cracks in continuous longitudinal butt welded joints to connect bottom plates to core plates,
(c) Cracks at the intersection of longitudinal ribs and transverse floor beam webs.

Strain distributions of the hollow deck in x- and y-directions on the upper sur-
face of the top plate at three loading cases A, B and C as shown in Fig. 2, are
indicated in Fig. 9 and those on the lower surface of the bottom plate are shown
in Fig. 10.

In Fig. 9, the highest strain in x-direction on the top plate occurred below the
applied load, and diminished rapidly close outside the region. Since it is evident
that the top plate is subjected to a large local out-of-plane bending, the fatigue
cracks will be initiated at the surface of the tension side of the top plate.
The fatigue fracture surface as seen in Fig. 7 indicates developing process of
this crack. The bottom plate is subjected to axial forces in the direction paral-
lel to the longitudinal weld line
to connect a bottom plate to core
plates, due to overall bending as
the whole structure.

Then, in order to obtain stress
conditions at the intersections of
longitudinal ribs and transverse
floor beam webs, the orthotropic
deck structure was replaced by a
three-dimensional model as assem-
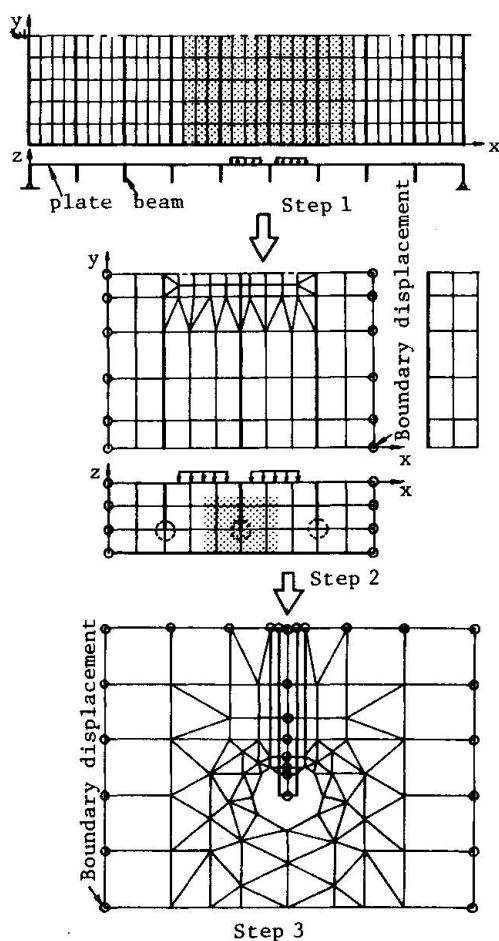blage of thin plates for analysis
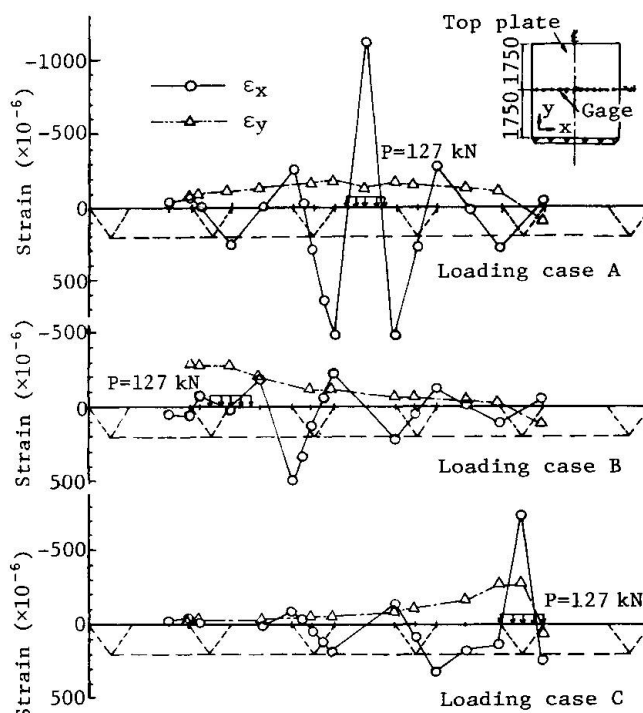by the finite element method.

Fig. 9 Strain distributions in top plate

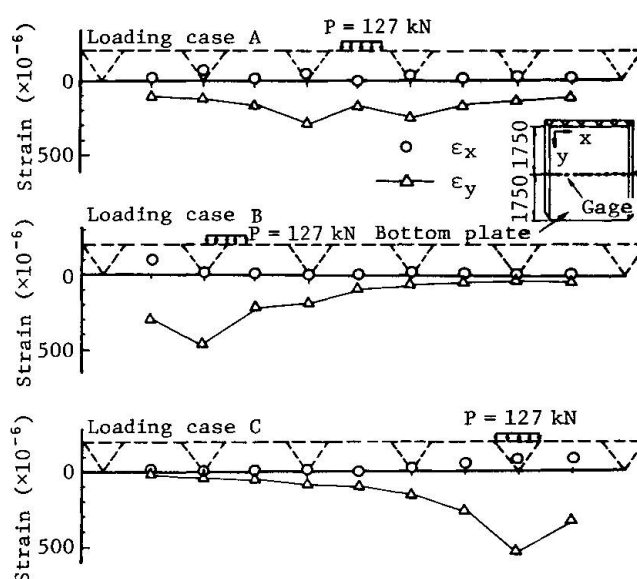Fig. 11 Finite mesh divisions
         at zooming step

Fig. 10 Strain distributions
         in bottom plate

The finite mesh divisions in each step
in the analytical procedure by a zoom-
ing method are shown in Fig. 11.
A plate element in which out-of-plane
and in-plane deformations were consid-
ered, and a beam element in which an
eccentricity between the middle sur-
face of the plate and the neutral axis
of the beam was considered, were used
for finite elements in a computer
program developed by the authors [4].

Fig. 12 Bending condition in
floor beam web

The analytical results indicate that
the floor beam web is subjected to not
only in-plane forces due to beam
actions, but also out-of-plane forces due to
flexural deformations of the longitudinal ribs
as shown in Fig. 12. Principal stress distribu-
tions on the outer surface of the floor beam web
are shown in Fig. 13. It is evident that there
are high stress concentrations at the upper part
of a circular cutout where a fatigue crack was
initiated.

Fig. 13 Principal stresses
in floor beam web

Figure 14 shows a comparison between stress
ranges for the cases A and C at a gage point on
a core plate. It is seen from this figure that
the core plate is subjected to stress reversal
as a load on the top plate moves from the center
of a V-shaped rib to the part between two
V-shaped ribs. When the vehicle load moves in
the direction perpendicular to the longitudinal
V-shaped rib as illustrated in Fig. 12, the
stress range in the fillet welded joint between
core plate and a top plate due to such stress
reversals becomes larger than that caused by
loading only at single position in the labora-
tory. Therefore, this part may become a weak
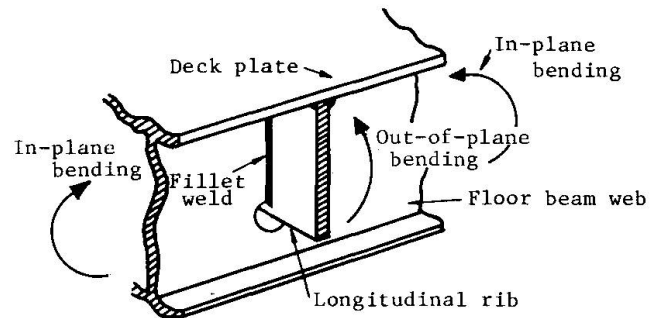point for fatigue failure under actual vehi-
cles.

$\sigma_r = -154$ MPa at case (A) (Compression)

$\sigma_r = 102$ MPa at case (C) (Tension)
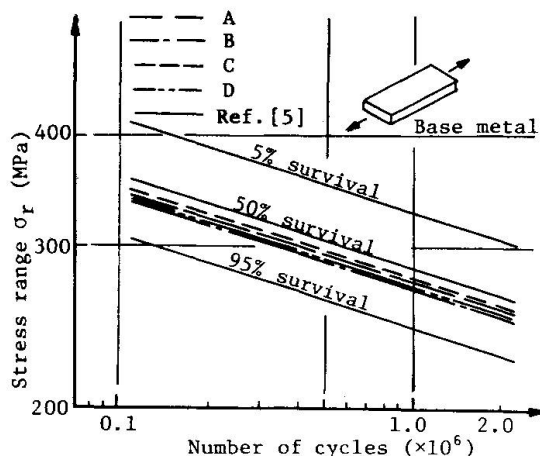
Fig. 14 Reversal of stress
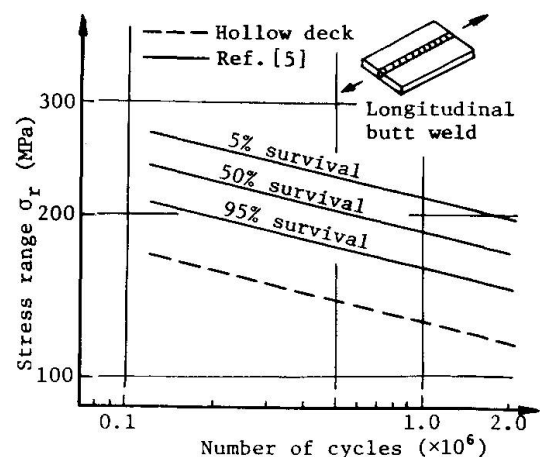
Fig. 15 S-N curves for base metal

Fig. 16 S-N curves for butt
welded joint

3.2 Comparison of Fatigue Strength

The present test results are compared with
the fatigue test data given by other investi-
gators for small coupon-type specimens sub-
jected to axial tensile stresses. Comparison
of S-N curves for the base metal is shown in
Fig. 15. In this figure, the solid line indi-
cates the P-S-N curves given by other inves-
tigators [5], and the lines A and B indicate
S-N curves for orthotropic deck panels and
the lines C and D for a hollow deck panel,
which have been obtained on the basis of the
present test results. Because the present
test data were insufficient to draw S-N
curves, these S-N curves were estimated on
the assumption that the slope is equal to
that of the P-S-N curves given by the other
investigators and cumulative fatigue damages
for a step loading can be evaluated by the
Miner's rule. It may be said that the fatigue
strength of the deck plate could be estimated
from the fatigue test data of the base metal
obtained by other investigators on coupon-
type specimens.

Fig. 17   Macrosection of
butt weld

Fig. 18   S-N relations of fillet
welded joint

Figure 16 shows S-N diagram for longitudinal
butt welded joints. The S-N curve for the
hollow deck panel was estimated in the same
manner as the case of the base metal. It is
observed that the fatigue strength of the
hollow deck panel is lower than that given by
other investigators [5]. From the observation
of the fracture surface as shown in Fig. 8,
it is recognized obviously that this fatigue crack was initiated due to the lack
of penetration as seen in Fig. 17. Therefore, it may be implied that the fatigue
strength of these butt welded joints is decreased by the existing lack of pene-
tration in the joint.

The fillet welded joints at the intersections of longitudinal ribs and floor beam
webs can be regarded as the transverse load-carrying ones by considering the
stress conditions of the floor beam web. S-N relations between principal stress
ranges which were measured at an upper part of the circular cutout on the outer
surface of the floor beam web by using rosette strain gages and estimated number
of cycles to crack initiation, are indicated in Fig. 18. The solid line in this
figure is a S-N curve for transverse load-carrying fillet welded joints [6].
The plotted data are remarkably scattered mainly because of inaccurate estimation
of crack initiation. The fatigue strength of this joint may be at the most lower
than that of the S-N curve for coupon-type specimens due to the effect of imper-
fect shape of welding.

4. CONCLUSIONS

Main conclusions for fatigue characteristics of the test panels at the present
study are summarized as follows:
(a) The deck plate subjected directly to repeated vehicle loads has a high
fatigue strength similar to that of the base metal. Since, in practical traffic,
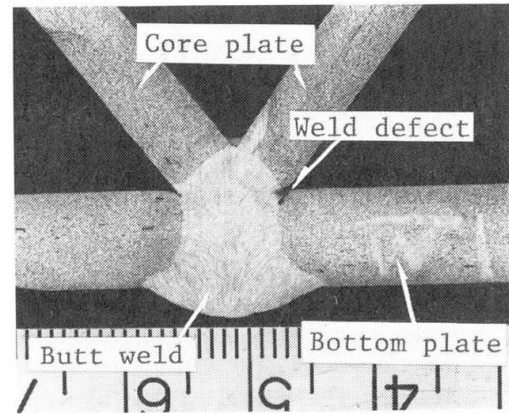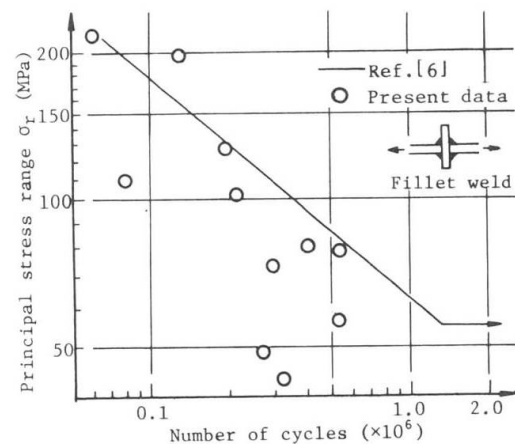the deck plate would not be used under severe loading conditions such as

laboratory fatigue tests, this plate will not be sustained critical fatigue damages.

(b) A fatigue crack at the longitudinal butt welded joint of the hollow deck was initiated from an 'internal' weld defect such as lack of penetration, while a fatigue crack at the transverse load-carrying fillet welded joint of the ortho-tropic deck was initiated from an 'external' weld defect such as imperfect shape of welding. Since the fatigue strengths of these welded joints are decreased due to weld defects, it will be necessary to take into account the reduction of fatigue strength at a detailed design. As a matter of general policy it should always be one of the aims for the fabrication of welded structures, to produce welds that are free from defects.

(c) When this hollow deck is placed in the traffic direction perpendicular to the longitudinal V-shaped ribs, the fillet welded joints between core plates and a top plate are always subjected to stress reversals. Since those joints will become a weak point for fatigue failures under actual vehicle loadings, it is necessary to examine the fatigue strength of those joints subjected to the stress reversal.

REFERENCES

1. Engineering News Record, Vol.17, Nov. 18, 1971, p.17.
2. MAEDA, Y., SERA, M. and UMESHITA, K. : Study on Fatigue of Orthotropic Steel Deck with Open-Shaped Longitudinal Ribs, Proceedings of 35th Annual Meeting of the Japan Society of Civil Engineers, Section-I, Sept., 1980, pp.201-202. *(in Japanese)*
3. MAEDA, Y., SURUGA, T. and KUSHIDA, K. : Application of Prefabricated Hollow Steel Decks to Bridge Constructions, Transportation Research Record No.665, Transportation Research Board, Sept., 1978, pp.155-163.
4. MAEDA, Y. and SERA, M. : Finite Element Method Analysis for Steel Plate Decks of Bridges, Technology Reports of the Osaka University, Vol.29, No.1514, Oct., 1979, pp.523-532.
5. SHIRAISHI, T. : A Fatigue Manual for Welding Designers, Welding Technique, March, 1964, pp.44-52. *(in Japanese)*
6. Society of Steel Construction of Japan : Fatigue Date Sheet, 1968, p.37. *(in Japanese)*

Fatigue Strength of Field-Welded Rib Joints of Orthotropic Steel Decks

Résistance à la fatigue des joints de raidisseurs soudés au montage des tabliers métalliques orthotropes

Ermüdungsfestigkeit von montagegeschweissten Versteifungsrippen orthotroper Fahrbahnplatten

A. KONDO
Assistant
Nagoya University
Nagoya, Japan

K. YAMADA
Assistant Prof.
Nagoya University
Nagoya, Japan

Y. KIKUCHI
Professor
Nagoya University
Nagoya, Japan

K. MIYAGAWA
Chief Manager
Topy Industries, Ltd.
Tokyo and Toyohashi, Japan

H. AOKI
Chief Manager
Topy Industries, Ltd.
Tokyo and Toyohashi, Japan

SUMMARY
The field-welded trough ribs of orthotropic steel decks may be susceptible to fatigue due to the unfavorable welding conditions. Fatigue tests are carried out on tensile and bending specimens of the decks with trough ribs. Both specimens contain joints butt-welded in overhead position with the backing strips at the center. The misalignment of the ribs and the lack-of-fitof the backing strips are also introduced to the specimens. Fatigue test results show the possible reduction of the fatigue strength.

RESUME
Les radisseurs en auge soudés au montage des tabliers métalliques orthotropes peuvent être sensibles à la fatigue due à des conditions de soudage défavorables. Des essais de fatigue ont été effectués sur des échantillons de tabliers raidis par des auges, sollicités à la traction et à la flexion. Les deux échantillons contiennent des joints soudés bout à bout en position renversée avec les couvre-joints au centre. Le mauvais alignement des raidisseurs et le manque de précision des couvre-joints ont aussi été introduits dans les échantillons. Les résultats des essais de fatigue montrent la réduction à apporter pour la résistance à la fatigue.

ZUSAMMENFASSUNG
Montagegeschweisste Hohlrippen orthotroper Fahrbahnplatten können infolge der ungünstigen Schweissbedingungen ermüdungsempfindlich sein. Es wurden Ermüdungsversuche an Fahrbahnplatten-Ausschnitten mit geschweissten Rippen unter Biege- und Zugbeanspruchung durchgeführt. Die Prüfkörper wurden über Kopf geschweisst und enthalten einen Längsstoss in der Mitte. Der Effekt des schlechten Ausrichtens der Rippen sowie die mangelhafte Ausführungsgenauigkeit beim Stoss mit Zusatzblech wurden bei den Prüfkörpern berücksichtigt. Ergebnisse aus diesen Ermüdungsversuchen zeigen eine mögliche Reduktion der Ermüdungsfestigkeit auf.

1.   INTRODUCTION

Trapezoidal trough closed ribs are increasingly used to stiffen the orthotropic steel decks of the medium to long span bridges in Japan. This system is economical due to the effective use of their bending stiffness and tortional rigidity. Moreover, amount of fillet welds and painting can be reduced compared with the open rib systems [1].

The orthotropic steel deck panels are often welded together on the erection sites. After connecting the steel deck plates, the trough ribs are normally butt-welded with backing strips. This system have advantage over the conventional bolted connections because it is simple in detail and can be air-proof. However, some engineers point out that the field-welded closed ribs may be susceptible to fatigue for the following reasons: 1) It is subjected to weld defects due to the unfavorable welding positions; 2) the misalignment of the closed rib cannot be corrected by itself, because the final profile is mainly determined by the profile of the deck; 3) out-of-fitness of the backing strip is often anticipated; and 4) tensile residual stresses are induced at the connection [3].

This report deals with the fatigue test results of tensile specimens and bending specimens of decks with trapezoidal trough ribs. Both specimens have the butt-welded joints with backing strips at the center. The welding is carried out in various positions to simulate the field welding of the trough rib joints. The misalignment of the ribs and the out-of-fitness of the backing strips are also introduced to the specimens.

2.   TEST SPECIMENS AND FATIGUE TESTS

The dimensions and the type of the tensile fatigue test specimens with groove welds are shown in Figure 1. The welding is carried out in the same way as the field welding of the trough rib joints. A series of specimens A and B are cut-out from the side and the bottom of the trapezoidal trough ribs, respectively. The specimens D are welded with rusted backing strips. The backing strips are intentionally placed 1 mm apart in one side. The specimens E contain stop and restart welds at the middle. Both specimens D and E are welded in overhead position. The specimens C are control specimens welded in flat position. Low hydrogen type electrodes of 3.2 mm diameter are used for all manual groove welds. Root opening of 5 mm and 45 degrees of bevel angle are maintained for all specimens.
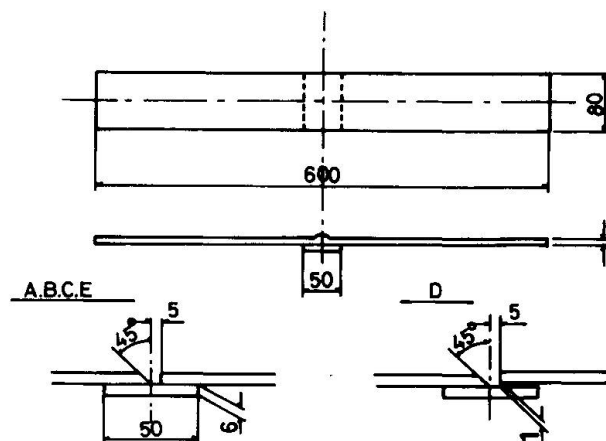
Series	Chracteristic
A	Specimens cut out from the side of full scale U-Section closed rib (Welded vertical)
B	Specimens cut out from the bottom of full scale U-Section closed rib (Welded in overhead position)
C	Control specimens welded in flat position
D	Specimens with out-of-straitness welded in overhead position. Rusted backing strip is used.
E	Specimens welded in overhead position with stop and re-start weld at the middle

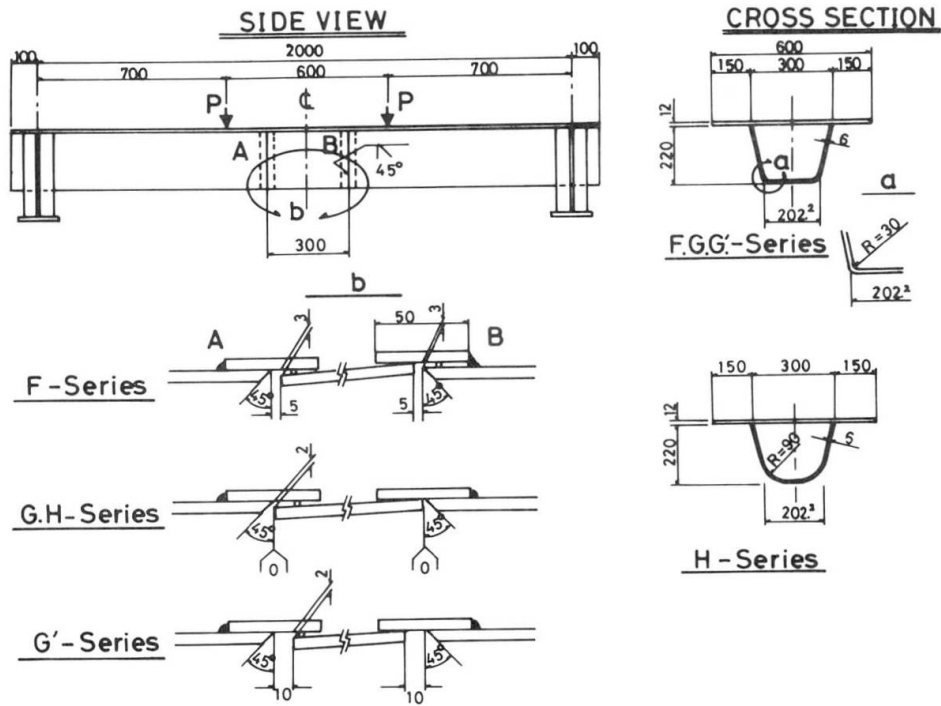Figure 1:   Tensile fatigue test specimens

Figure 2:   Bending fatigue specimens of decks with trapezoidal trough ribs.

The bending deck specimens with trapezoidal trough ribs are shown in Figure 2. The trough ribs are cold-formed from a flat plate of 6 mm thick by press. The radius of the corner of 30 mm (5 times the rib thickness) is used for the specimens F, G and G', while that of 90 mm (15 times the rib thickness) is used for the specimens H. Butt welding is carried out with low hydrogen type electrodes of 3.2 mm diameter in overhead position with engine driven welding machine. The welding process simulates the field welding. The specimens are first fabricated in the designated form. The center part of the ribs is left open. The ends of the ribs are bevelled to 45 degrees. Then the connecting ribs of 300 mm long is placed at the position to fill the gap with the tack welding. The out-of-fitness and the root opening, which are intentionally introduced to each specimen, are shown in Figure 2. The steels used to fabricate the specimens conform to JIS SS41 steel, equivalent to ASTM A36. The test set-up for the bending fatigue tests is shown in Photo 1.
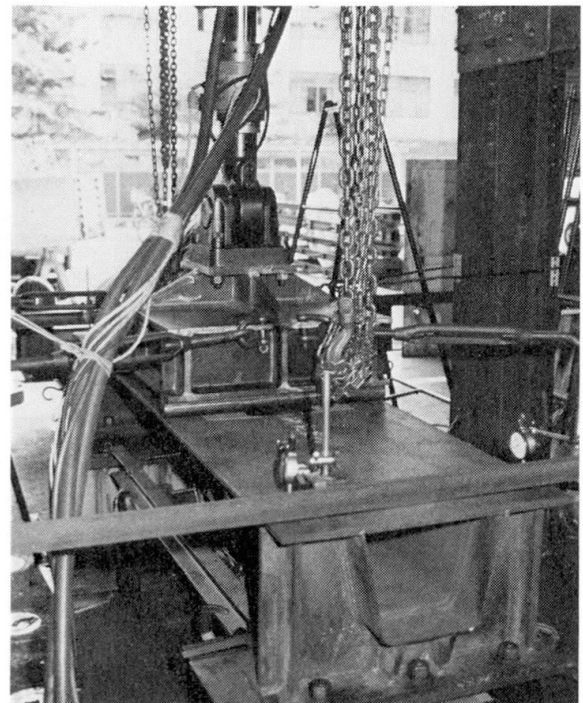

Photo 1:   Test set-up for bending fatigue test.

3.   FATIGUE TEST RESULTS

3.1   Fatigue Test Results of Tensile Specimens

Fatigue test results of all 44 tensile specimens are plotted in Figure 3. Fourteen (14) specimens did not fail over 3 million cycles and the fatigue tests are discontinued. The data is shown by the symbols with arrow. The fatigue crackings mainly initiate at the weld root of the specimens A, B and D, as shown in Fig. 6. This is due to the unfavorable root condition introduced by the welding in overhead position. Specimens E are also welded in overhead position, but the fatigue cracks initiate from the toe near the stop and restart posision.

Although wide scatter of the data is observed for all types of the specimens, the specimens D show the lowest fatigue strength. The mean regression line of the specimens D is plotted by the dotted line in Figure 3, while that of the specimens A, B, C and E together is plotted by the solid line for comparison. The average fatigue strength at $2 \cdot 10^6$ cycles of the specimen D is about 90 MPa, while that for the specimens A, B, C and E together is about 115 MPa.

Prior to the fatigue tests of the tensile specimens, all specimens are examined through X-ray radiography. The observation is then classified according to the Japanese Industrial Standards (JIS Z-3104), as shown in Figures 4 and 5. First, Figure 4 shows the type of defects observed in the tensile specimens. About 80 percent of the specimens A, B and D welded in overhead and vertical positions show some sorts of weld defects, while only 20 percent of the specimens show the defects when welded in flat position. It is speculated that the unfavorable welding conditions, which must be reluctantly accepted for welding the trough rib joint in the field, leave more or less weld defects.

Then the specimens are also classified into four degrees of severeness of weld defects depending upon the number and the size of the internal defects. The welded joints with the third and fourth degree of weld defects are not acceptable, and must be repaired, for tension members of the highway bridges [2]. As shown in Figure 4, the acceptability of the weldments is greatly affected by the welding position. About half of the specimens D show the weld defects more than third degree and are not acceptable for welding the trough rib joints.
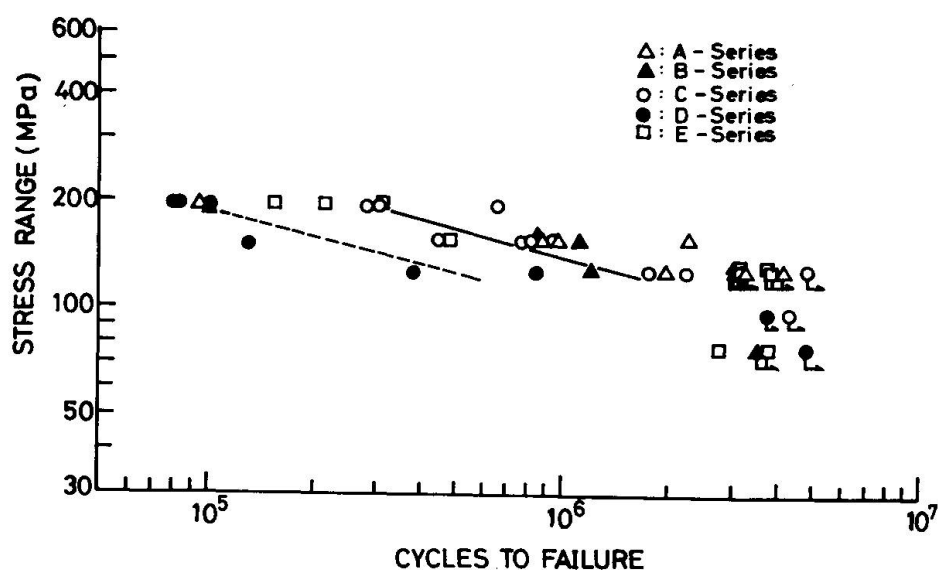

Figure 3:   Fatigue test results of tensile specimens.

It should be noted that the radiographic examination of the field welded trough rib joints is not applicable. Therefore, the soundness of the welds may be achieved through the quality control of the welding process, such as controlling the out-of-fitness of the backing strip, cleaning the surface, controlling the root opening, training the welders, and so on.

Fatigue test results are replotted in accordance with the degree of the internal defects in Figure 6. It seems that the degree of the severeness of the internal defects affect little to the fatigue strength of the specimens. This may be due to the fact that the fatigue cracks mainly initiate and propagate from the weld toes or from the weld roots, as shown in the insert of Figure 6. The fatigue crackings from these places are supposed to be almost independent from the existance of internal defects.

Similar groove-welded tensile specimens with backing strips are also tested at the Public Works Research Institute, Ministry of Construction [3]. The parameter of the tests include the qualification of the welders, the shape of the groove face, the out-of-fitness of the backing strips, the unfavorable welding positions and the weld defects. Out of 22 specimens tested, ten (10) specimens have the root opening of 5 mm and the bevel angle of 45 degrees, comparable to the present study. These fatigue test results are also plotted by the inverse triangular in Figure 6. As the results of the X-ray radiography, eight specimens show the fourth degree of weld defects, while two others show the first degree. The effect on the degree of the severeness of the weld defects on the fatigue life also seems negligible, and the data is generally in good agreement with the present test results.
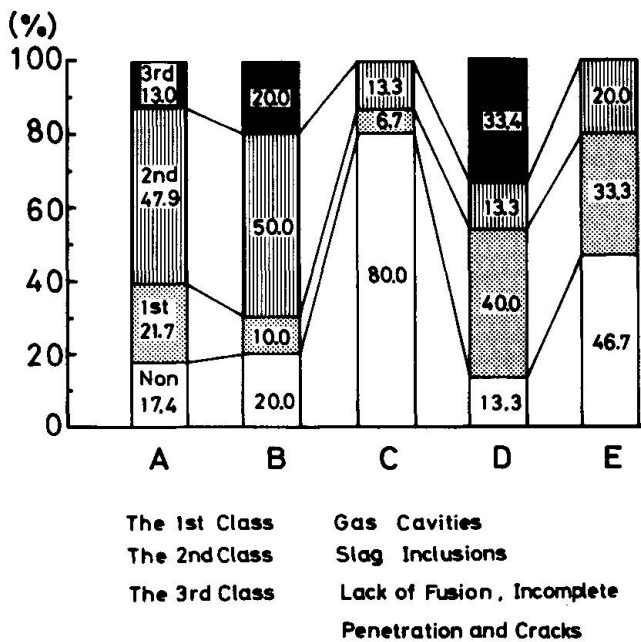

Figure 4: A kind of weld defects observed by the X-ray radiography.

The 1st Class   Gas Cavities
The 2nd Class   Slag Inclusions
The 3rd Class   Lack of Fusion, Incomplete
                  Penetration and Cracks
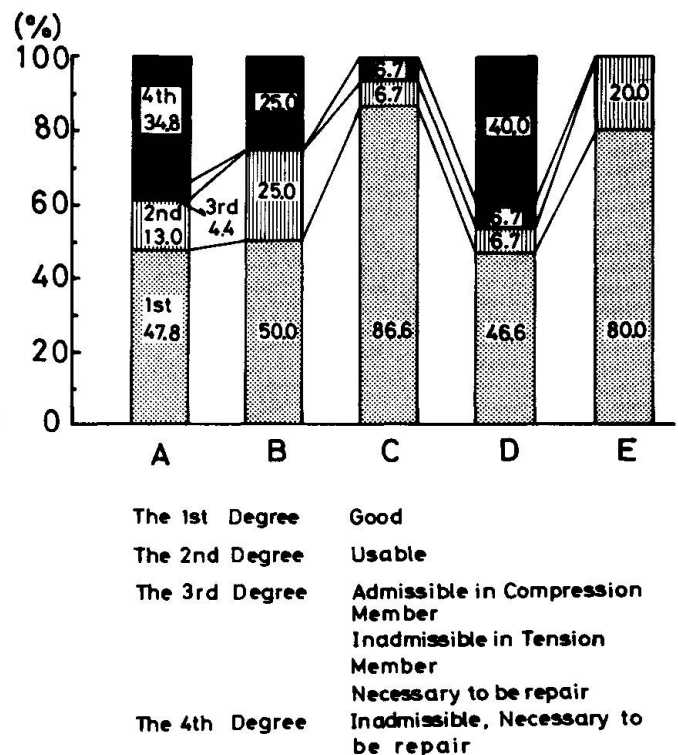
Figure 5: Classification of the severeness of the weld defects for each type of specimens.

The 1st Degree   Good
The 2nd Degree   Usable
The 3rd Degree   Admissible in Compression Member
                  Inadmissible in Tension Member
                  Necessary to be repair
The 4th Degree   Inadmissible, Necessary to be repair

Series	No.	Starting Point of Crack		
		Root	Toe	Both
A	7	5	1	1
B	8	6	2	
C	12	1	10	
D	8	6	1	1
E	9		9	

O   The 1st Degree(▽)
△   The 2nd Degree
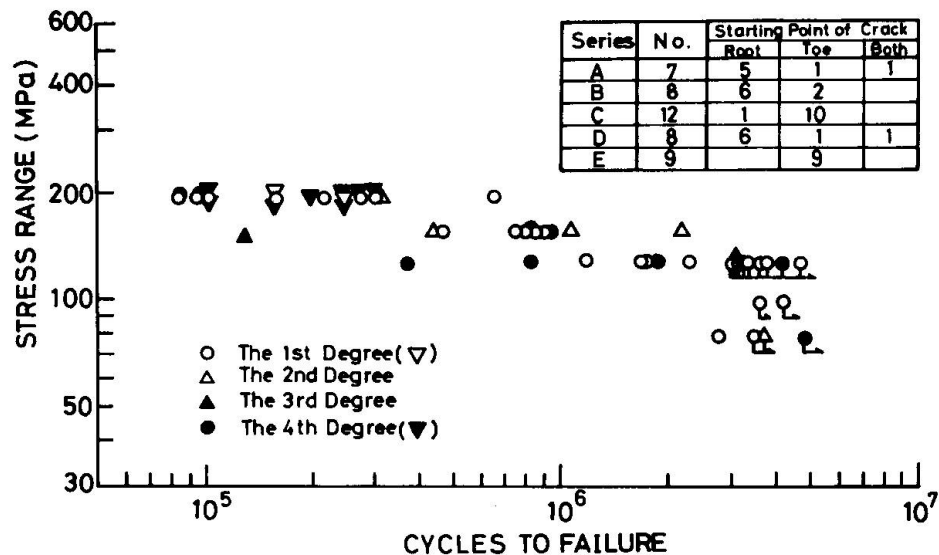▲   The 3rd Degree
●   The 4th Degree(▼)

Figure 6:   Summary of tensile fatigue test results
according to the severeness of the weld defect.

3.2   Bending Fatigue Test Results of Decks with Trough Ribs

Fatigue test results of decks with trough ribs are plotted in Figure 7. Stress ranges correspond to the nominal stress at the bottom fiber of the ribs, and the number of cycles to failure corresponds to the cycles at the complete separation of the rib joints.

Total of 17 specimens are tested. The specimen H tested at the stress range of 83 MPa shows no fatigue cracking after 4 million cycles, and the test is discontinued. For one specimen G tested at 59 MPa, fatigue cracks are observed at $3.45 \cdot 10^6$ cycles, and the test is continued up to 5 million cycles. The cracks propagate to almost half the bottom flange of the rib.

▲   F – Series
●   G – Series
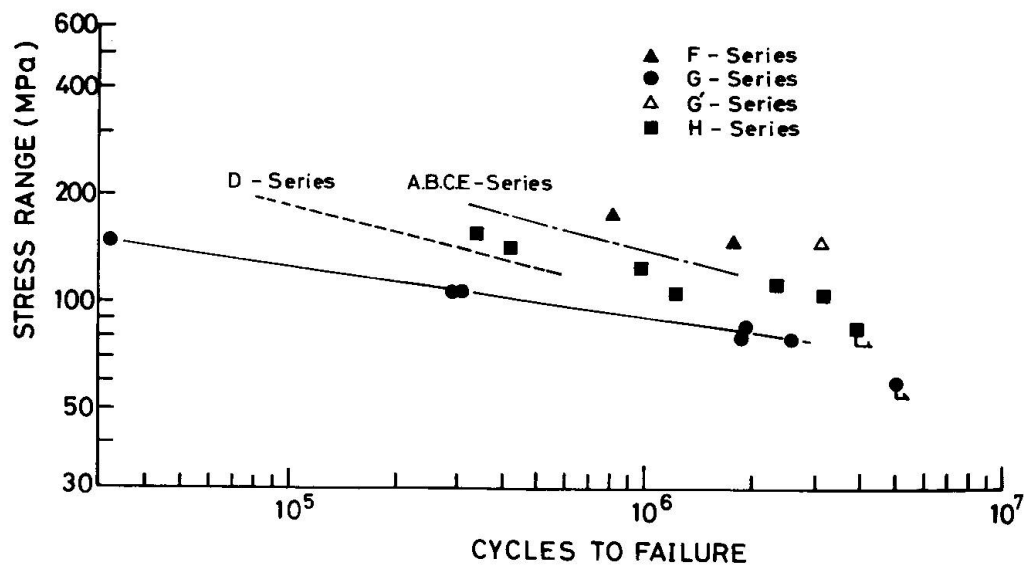△   G′ – Series
■   H – Series

Figure 7:   Bending fatigue test results of all 17 specimens
of decks with trough ribs.

The fatigue cracks initiate and propagate from the root of the groove welds in 14 specimens. A typical fatigue fracture surface of the specimen is shown in Photo 2. The cracks penetrate the groove welds from inside to outside and are first observed at the surface of the groove welds at the bottom of the trough ribs. Then the cracks propagate gradually in two directions to separate the bottom flanges of the trough ribs completely. The specimen F tested at the stress range of 147 MPa shows the fatigue cracking from the toe of the tack welding of the backing strip.

As shown in Figure 2, the root opening of the specimens G and H is zero, so that it seems difficult for the welders to achieve the complete penetration of the groove welds, especially in overhead position. For six specimens G and four specimens H, fatigue failures occur from the incomplete penetration of the side B (see Figure 2), where no misalignment of the trough ribs is introduced. The incomplete penetration of about 1 mm deep is clearly found at some of the fatigue fracture surface.

Two specimens tested at the stress ranges of 125 MPa and 147 MPa have fatigue cracking from the side A, where 2 mm of misalignment of the trough ribs is maintained (see Figure 2). Fatigue cracks initiate and propagate from the root of the groove welds, where the sudden change of the section due to the mis-alignment exists. No incomplete penetration is visible on the fracture surface of these specimens. Fatigue cracks of the specimens F and G' also initiate and propagate from the weld root of the side A. It seems that the weld roots near the backing strips is still the initiation point of the fatigue cracks due to incomplete penetration or defects. Fatigue life is, however, prolonged for these specimens probably because the root opening of more than 5 mm make it easy to groove-weld and also reduces the degree of sudden change of the section, compared with the specimens G and H.
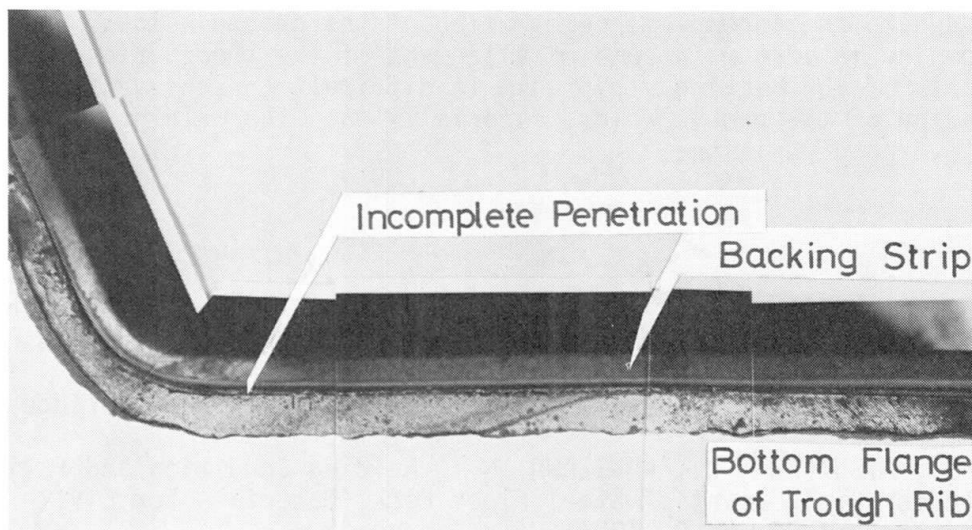
Photo 2: Typical fatigue fracture surface of trough rib joints.

Obviously the incomplete penetration of the groove welds can be the initiation point of fatigue cracking, or can be almost initial cracks as it is. This lowers the fatigue strength of this detail. Consequently, the specimens G show the lowest fatigue strength, as shown in Figure 7. A mean regression line of the specimens G is computed and plotted by the solid line for comparison. The average fatigue strength at $2 \cdot 10^6$ cycles is about 80 MPa. This is even lower than that of the tensile specimens D plotted by the dotted line. When the full penetration of the groove welds is maintained with sufficient root opening,

such as for the specimens F, the fatigue strength is even longer than that of the tensile specimens A, B, C and E together.

The fatigue strength is somewhat higher when the radius of 90 mm is used at the corner of the trough ribs, such as for the specimens H. The specimens G and H are fabricated at two different occasions by the different welders. From visual inspection of the fatigue fracture surfaces, the specimens H are found to have less amount of the incomplete penetration than the specimens G. The radius of 5 times the thickness of the ribs (or 30 mm for the 6 mm thick ribs) is normally used for the corner of the trough ribs [4].

4.   SUMMARY

The fatigue tests of the butt-welded tensile specimens and the bending specimens are carried out to obtain the fatigue strength of the field-welded trapezoidal trough ribs of the orthotropic steel decks. The groove welds with the backing strips in overhead position simulate the field welding conditions of this type of details. The followings summarize the findings.
1)   The fatigue tests of the groove-welded tensile specimens show that the specimens failed from either weld toe or weld root. The specimens D, which contain the misalignment of about 1 mm and are welded in overhead position with rusted backing strips, show the lowest fatigue strength.
2)   As the results of the X-ray radiography of the tensile specimens, the internal defects are introduced to the joints largely by the unfavorable welding position, and/or the rusted backing strips.
3)   However, the internal defects seems to have little effect on the fatigue strength of the tensile specimens.
4)   From the bending fatigue tests of the decks with trough ribs, fatigue crackings are observed mainly from the root of the groove weld. Reduction of the fatigue strength is significant when root opening is zero. This may be due to the incomplete penetration of the groove welds. When the root opening is zero with some misalignment of the trough ribs and out-of-fitness of the backing strips, it is difficult to achieve the complete penetration of the groove welds, especially when the welding is carried out in overhead position.

REFERENCES

[1] WATANABE, N., OSHIMA, H.: Investigation of Design Examples and Economical Design for Orthotropic Steel Decks, The Bridge and Foundation Engineering, Vol. 10, No.9, 1976. (In Japanese)
[2] JAPAN ROAD ASSOCIATION: Standard Specification for Highway Bridges, 1980, 2.
[3] SAEKI, S., NISHIKAWA, K., KAKIZAWA, N.: Welding Condition and Fatigue Strength for Field Joint of Steel Floor Deck, Materials for Civil Engineering, Vol.23, No.8, 1981. (In Japanese)
[4] JAPAN SOCIETY OF CIVIL ENGINEERS: Design Rules of Orthotropic Steel Decks for Honshu-Shikoku Bridges, 1978, 3.